MCB
Journals.ASM.org

Reactive Oxygen Species-Mediated DJ-1 Monomerization Modulates Intracellular Trafficking Involving Karyopherin β2

Benny Björkblom,[a,b]* Jodi Maple-Grødem,[a,b] Marc Rhyan Puno,[c] Mark Odell,[c] Jan Petter Larsen,[a] Simon Geir Møller[a,d]

The Norwegian Center for Movement Disorders, Stavanger University Hospital, Stavanger, Norway[a]; Center for Organelle Research, University of Stavanger, Stavanger, Norway[b]; Department of Molecular and Applied Biosciences, University of Westminster, London, United Kingdom[c]; Department of Biological Sciences, St. John's University, New York, New York, USA[d]

Mutations in DJ-1 are a cause of recessive, early-onset Parkinson's disease (PD). Although oxidative stress and mitochondrial integrity have been implicated in PD, it is largely unknown why neurons degenerate. DJ-1 is involved in oxidative stress-mediated responses and in mitochondrial maintenance; however, its specific function remains vague. Here we show that DJ-1 exhibits neuronal dynamic intracellular trafficking, with dimeric/monomeric cycling modulated by the oxidative environment. We demonstrate that oxidative stress enhances monomerization of wild-type cytosolic DJ-1, leading to nuclear recruitment. The pathogenic DJ-1/E163K variant is unable to homodimerize but is retained in the cytosol upon wild-type DJ-1 heterodimerization. We found that this wild-type/pathogenic heterodimer is disrupted by oxidative stress, leading to DJ-1/E163K mitochondrial translocation. We further demonstrated that endogenously expressed wild-type DJ-1 is imported into neuronal nuclei as a monomer and that nucleo-cytoplasmic transport is oxidative stress mediated. We identified a novel proline-tyrosine nuclear localization signal (PY-NLS) in DJ-1, and we found that nuclear monomeric DJ-1 import is mediated by an oxidative stress-dependent interaction with karyopherin β2. Our study provides evidence that oxidative stress-mediated intracellular trafficking of DJ-1, mediated by dynamic DJ-1 dimeric/monomeric cycling, is implicated in PD pathogenesis.

Parkinson's disease (PD) is a progressive neurodegenerative disorder that is neuropathologically characterized by a relatively selective loss of dopaminergic (DA) neurons and the presence of Lewy bodies in the substantia nigra. The majority of PD cases are sporadic; however, early-onset PD, often monogenic in nature, accounts for between 5 and 10% of all cases (1). Autosomal recessive forms of early-onset PD are caused by mutations in parkin (PARK2) (2), PTEN-induced putative kinase 1 (PARK6; PINK1) (3), and Parkinson protein 7 (PARK7; DJ-1) (4).

DJ-1 belongs to the Thi/PfpI protein superfamily and is expressed in a variety of tissues, including the brain (5). DJ-1 has an atypical peroxiredoxin-like peroxidase activity that is involved in scavenging mitochondrial H_2O_2, and DJ-1 knockout mice have increased mitochondrial H_2O_2 levels (6, 7). DJ-1 shifts toward a more acidic isoelectric point in response to reactive oxygen species (ROS) (8, 9), and DJ-1 knockout models show increased sensitivity toward oxidative stress/mitochondrial toxins (9–13). Conversely, overexpression of wild-type (wt) DJ-1 protects cells against ROS/mitochondrial toxins (9, 14). DJ-1 harbors three cysteine residues (C46, C53, and C106); C106 oxidizes to form a cysteine-sulfinic acid, and C106 mutations lead to DJ-1 loss of function (7, 10, 15).

DJ-1 localizes to the cytoplasm, nucleus, and mitochondria (7, 16, 17). Mitochondrial DJ-1 translocation is enhanced by oxidative stress, and C106 oxidation is necessary for translocation (7). Targeting of DJ-1 to mitochondria protects cells against oxidative stress (18), and DJ-1 may maintain complex I activity (19). The precise mechanism of mitochondrial translocation is not fully understood, but various DJ-1 mutants, unable to homodimerize, preferentially localize to mitochondria (20). DJ-1 also associates with multiple RNA targets, including mitochondrial genes and glutathione metabolism genes, suggesting that the DJ-1 pleiotropic effects are due to binding to multiple RNAs (21, 22).

In the nucleus, DJ-1 sequesters the death protein Daxx, preventing it from entering the cytoplasm, leading to loss of activation of Ask1 and thus preventing cell death (23). In the nucleus, DJ-1 can also act as a coactivator of various pathways (24, 25). DJ-1 also leads to Nrf2 instability that results in a deficit in expression of detoxification enzymes (26). DJ-1 has also been shown to interact with p53, modifying its activity (27, 28). DJ-1 can regulate the tyrosine hydroxylase promoter and thus influence dopamine production (29, 30).

Although it is clear that DJ-1 function is through oxidative stress-mediated responses within a framework of subcellular localizations, the molecular mechanisms underlining this remain vague. Here, we provide new insights into dynamic intracellular trafficking of DJ-1 in response to oxidative stress. We show that oxidative stress enhances monomeric forms of wt DJ-1 and of DJ-1 E163K, leading to nuclear and mitochondrial recruitment, respectively. We further show that monomeric DJ-1 translocates to the nucleus via a nonclassical proline-tyrosine nuclear localization signal (PY-NLS) domain and that this is mediated by karyopherin β2, which interacts with DJ-1 in an oxidation-dependent fashion. Combined, our data suggest that cytoplasm-mitochondrion DJ-1 trafficking and cytoplasm-nucleus DJ-1 traffick-

Received 26 February 2014 **Returned for modification** 25 March 2014
Accepted 1 June 2014

Published ahead of print 9 June 2014

Address correspondence to Benny Björkblom, benny.bjorkblom@chem.umu.se, or Simon Geir Møller, mollers@stjohns.edu.

* Present address: Benny Björkblom, Department of Chemistry, Umeå University, Umeå, Sweden.

doi:10.1128/MCB.00286-14

ing involve dynamic cycling between dimeric and monomeric DJ-1 states that are dependent on the oxidative environment.

MATERIALS AND METHODS

Antibodies and reagents. Anti-green fluorescent protein (anti-GFP; JL-8) and rabbit full-length polyclonal anti-GFP (632460) antibodies were obtained from Clontech (Mountain View, CA). Antiactin (AC-40) and anti-DJ-1 (E2.1) mouse monoclonal antibodies were from Sigma-Aldrich (St. Louis, MO). Anti-c-Jun (60A8) was from Cell Signaling Technology (Beverly, MA). Anti-superoxide dismutase 1 (anti-SOD1; AB16831) and rabbit polyclonal antibody anti-karyopherin 2β (D45) were from Abcam (Cambridge, United Kingdom). Anti-DJ-1 (11681-1–alkaline phosphatase) rabbit polyclonal antibody was from the Protein-Tech Group (Chicago, IL) and anti-microtubule-associated protein (anti-MAP; AP20) was from Leinco Technologies (St. Louis, MO). The antibodies 632460 and 11681-1 were used for immunoprecipitation (IP). Anti-monomeric DJ-1 (S3618-2) was raised against human DJ-1 N-terminal residues 13 to 30 by using the synthetic peptide NH_2-GAEEMETV IPVDVMRRAG(C). The antibody was raised in rabbits by using peptide conjugated to keyhole limpet hemocyanin via an additional cysteine residue (in parentheses in the above sequence). S3618-2 was affinity purified after the fourth immunization boost. Rabbit monoclonal anti-DJ-1 (N01A) was a gift from Darren Moore (31). Anti-rabbit and anti-mouse horseradish peroxidase-conjugated secondary antibodies were from GE Healthcare. Complete phosphatase and protease inhibitor cocktail tablets were from Roche (Basel, Switzerland). Dynabeads, MitoTracker red, and anti-mouse and anti-rabbit Alexa Fluor 488/568-conjugated secondary antibodies were from Invitrogen Life Technologies (Paisley, United Kingdom). Hydrogen peroxide solution was from Sigma-Aldrich (St. Louis, MO). Mouse embryonic fibroblast (MEF) DJ-$1^{-/-}$ cells were obtained from Huaibin Cai (32).

Molecular cloning. For mammalian cell expression, the human *PARK7* gene was amplified with DJ1-F-XhoI (5′-ATCTCGAGATGGCT TCCAAAAGAGCTC-3′) and DJ1-R-KpnI (5′-AT GGTACCCTAGTCT TTAAGAACAAGTGG-3′) and inserted into pCDNA3.1(-) hygro (Invitrogen). For C-terminal fusion with either enhanced GFP (EGFP) or ptdTomato, *PARK7* was amplified using DJ1-F-XhoI and either DJ1-R1-KpnI (5′-ATGGTACCGTCTTTAAGAACAAGTGG-3′) or DJ1-R2-KpnI (5′-ATGGT ACCGCGTCTTTAAGAACAA GTGGAGC −3′) and cloned into pEGFP or ptdTomato (Clontech), respectively. For fusion of DJ-1 truncations to EGFP, each fragment was amplified with DJ1-F-XhoI and either DJ1-SP-1 (5′-ATGGTACCGACATCTACAGGGATGACC-3′), DJ1-SP-2 (5′-ATGGTACCGACCACATCACGGCTACAC-3′), DJ1-SP-3 (5′-ATGGTACCACCTCCTGGTAGAACCACC 3′), or DJ1-SP-4 (5′-AT GGTACCGCCCTTCCGGTTTTCCTGC-3′) and cloned into pEGFP (Clontech). (Underlined portions of the sequences represent restriction sites.) *PARK7* point mutations were generated by site-directed mutagenesis. All constructs were verified by DNA sequencing. COX8-dsRed2 was a gift from Michael J. Courtney. TOM7-GFP was a gift from Mike Ryan (33).

Cell culture and transfections. Primary mouse cerebellar granule neurons were prepared from postnatal day 6 NMRI/BomTac mice as described previously (34). Neuronal cell survival was carried out by assessing the presence of pyknotic cell nuclei (35). Human neuroblastoma SHSY-5Y cells and MEF DJ-$1^{-/-}$ cells were cultured in Dulbecco's modified Eagle's medium supplemented with 10% heat-inactivated bovine calf serum, 2 mM glutamine, 1% nonessential amino acids (Sigma-Aldrich), 50 U/ml penicillin, and 50 μg/ml streptomycin (36). Cell survival upon H_2O_2 exposure was measured using a tetrazolium salt, WST-1 (Roche), according to the manufacturer's instructions and with a Thermo Scientific Multiskan Ascent apparatus at 450-nm wavelength and 630 nm as reference. All cell culture reagents were from Invitrogen Life Technologies (Paisley, United Kingdom). Primary mouse neurons were transiently transfected at 6 days incubation *in vitro* (DIV) with 1 μg/cm^2 plasmid DNA as described previously (37), but no kynurenate or D-APV was added and no dimethyl sulfoxide-glycerol shock was performed. DJ-1 knockout cells were transfected using Lipofectamine 2000 (Invitrogen Life Technologies).

Immunofluorescence imaging and acquisition. Mitochondria were stained with 50 nM MitoTracker for 30 min in culture medium. Immunocytochemical staining was carried out as described previously (35, 36). Briefly, following fixation, permeabilization, and blocking, samples were incubated overnight at 4°C with primary antibody. Alexa Fluor 488/568 fluorophore-linked secondary antibodies (4 μg/ml) were used for 1 h at room temperature (RT) prior to nuclear staining using 2 μg/ml Hoechst 33342 stain (Invitrogen) and mounting in Mowiol 4-88 mounting medium containing 2.5% (wt/vol) Dabco antifading reagent (Sigma-Aldrich). Images were taken using an inverted Nikon Ti A1R confocal laser scanning microscope. Excitations used laser lines at 408 nm, 488 nm, or 561 nm, and images were recorded at 425/475 nm, 500/550 nm, or 570/620 nm, respectively. Laser intensities/detection settings were kept constant between parallel images to enable sample comparisons. NIS-Elements imaging software 4.0 (Nikon, Japan) was used for image capture and measurement of fluorescence intensity.

Cell fractionations. Cells expressing DJ-1–GFP variants or TOM7-GFP were washed in phosphate-buffered saline (PBS), scraped off their growth support, centrifuged at 100 × *g* for 5 min, and resuspended in 4 volumes of isotonic sucrose buffer A (250 mM sucrose, 10 mM HEPES-KOH [pH 7.5], 1.5 mM $MgCl_2$, 10 mM KCl, 0.5 mM dithiothreitol) containing phosphatase/protease inhibitors. The cell suspension was sonicated on ice twice for 6 s at a 50% amplitude by using a Kontes KT 50 Micro ultrasonic cell disruptor. The cell suspension was centrifuged at 300 × *g* for 10 min at 4°C to remove unbroken cells, nuclei, and cell debris. The supernatant, containing total protein extract, was termed SN1. SN1 was centrifuged at 3,000 × *g* for 10 min at 4°C, and the pellet was washed once in sucrose buffer A and centrifuged at 3,000 × *g* for 10 min. The washed pellet, containing high-molecular-weight organelles, was termed P1. The supernatant from SN1 was centrifuged at 25,000 × *g* for 20 min at 4°C to obtain supernatant SN2, which contained soluble proteins, and a second pellet (P2) that contained low-molecular-weight organelles. P2 was washed once in sucrose buffer A and centrifuged at 25,000 × *g* for 20 min at 4°C. The washed P1 and P2 pellets were dissolved in sucrose buffer A (2% [vol/vol]) Triton X-100, 300 mM NaCl) prior to denaturation in SDS-PAGE sample buffer and protein analysis by Western blotting. Quantification was done using a ChemiDoc XRS apparatus (Bio-Rad) and Quantity One software.

Cell nucleus isolation. Isolation of nuclear and cytoplasmic cell fractions was carried out as described previously (38). Nuclear pellets were collected by centrifugation at 300 × *g* for 10 min at 4°C, repeatedly washed in hypotonic gentle lysis buffer without detergent, and collected by centrifugation. The total protein concentration for each fraction was measured by the Bradford method, and equal proportions of nuclear and cytosolic fractions were analyzed by native PAGE or denaturing SDS-PAGE.

Brain homogenization. Mouse brain tissue was collected from postnatal day 6 NMRI/BomTac mice or postnatal day 1, 7, or 21 and 6-month-old adult C3H mice after decapitation; samples were snap-frozen in liquid nitrogen and stored at −80°C. Human brain tissue was collected from the Stavanger University Hospital and processed according to the NYBB Columbia University method (39). For protein analysis, human brain areas were dissected from frozen coronal brain slices of a 78-year-old female with no neurological disease history. Each tissue sample was weighed and lysed in 10 volumes of ice-cold RIPA buffer (50 mM Tris-HCl [pH 7.4], 150 mM NaCl, 0.5% [wt/vol] sodium deoxycholate, 0.1% [vol/vol] SDS) containing protease inhibitor. Tissue was homogenized with an Ultra-Turrax instrument followed by membrane solubilization using 0.9% (vol/vol) IGEPAL-630 and incubation for 15 min on ice. The homogenates were precleared at 2,600 × *g* for 15 min at 4°C. The total soluble protein concentration was measured by the Bradford method and subjected to SDS-PAGE.

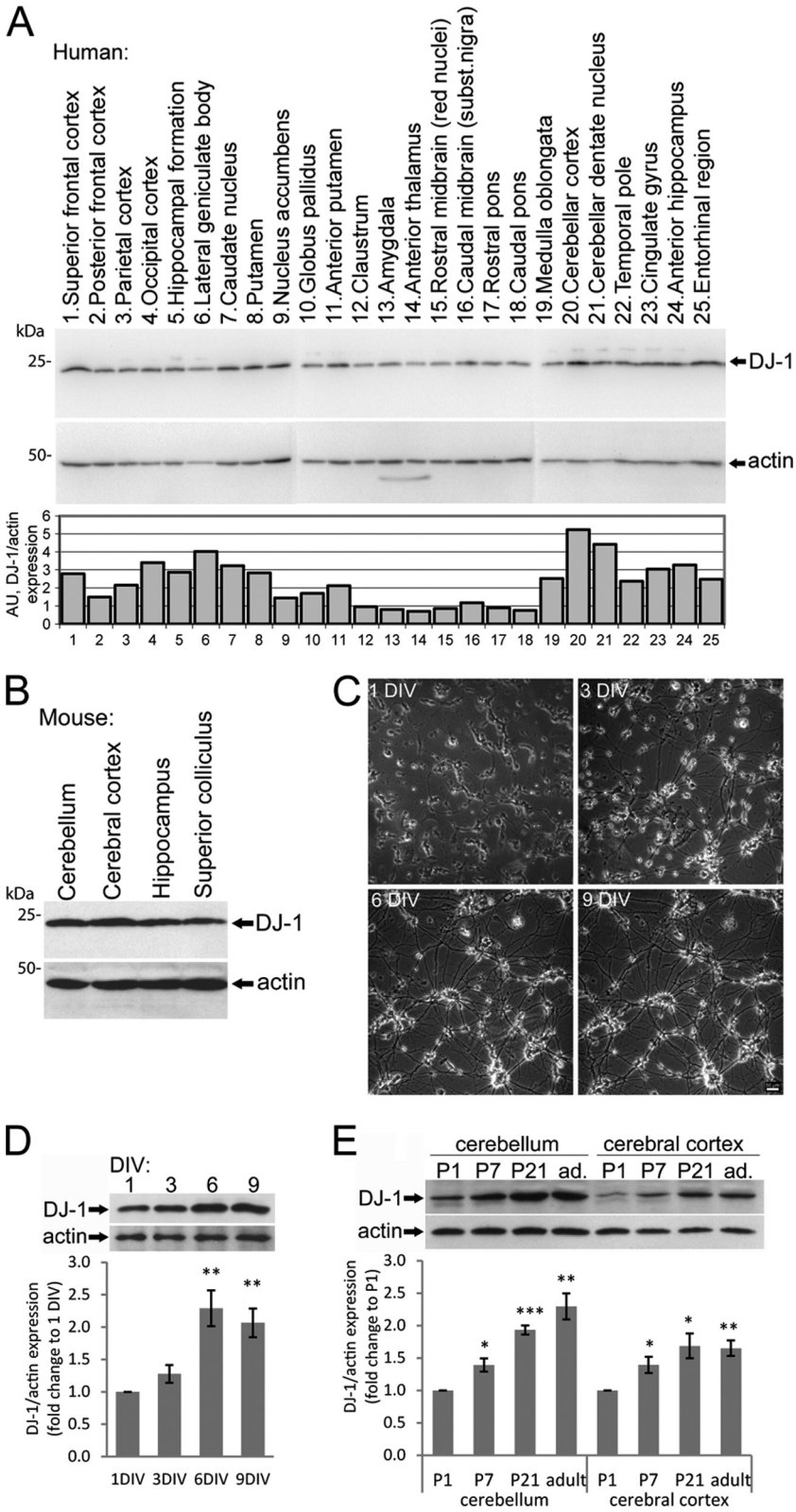

FIG 1 DJ-1 protein abundance is brain region specific and is regulated during neuronal development and neuritogenesis. (A) SDS-PAGE, quantitative Western blot analysis, and quantification of DJ-1 and actin protein expression in 25 selected human brain areas. AU, arbitrary units. (B) SDS-PAGE and Western blot analysis of DJ-1 and actin protein expression in different postnatal day 6 mouse brain areas. (C) Phase-contrast images of primary granule neurons in culture during development. The same cell growth area at 1 to 9 DIV is shown. Bar, 50 μm. (D) SDS-PAGE, Western blot analysis, and quantification of DJ-1 and actin protein expression in developing primary granule neurons at 1 to 9 DIV. Data shown are the fold change to 1 DIV. The means ± standard errors of the means (SEM) for three data sets are shown. **, $P < 0.01$. (E) SDS-PAGE, Western blot analysis, and quantification of mouse DJ-1 and actin protein expression in the cerebellum and cerebral cortex of developing juvenile (postnatal days 1, 7, and 21) and adult (ad., 6 months old) mouse brains. Data shown are the fold change, to postnatal day 1. The mean (±SEM) expression levels for three animals per age group are shown. *, $P < 0.05$; **, $P < 0.01$; ***, $P < 0.001$.

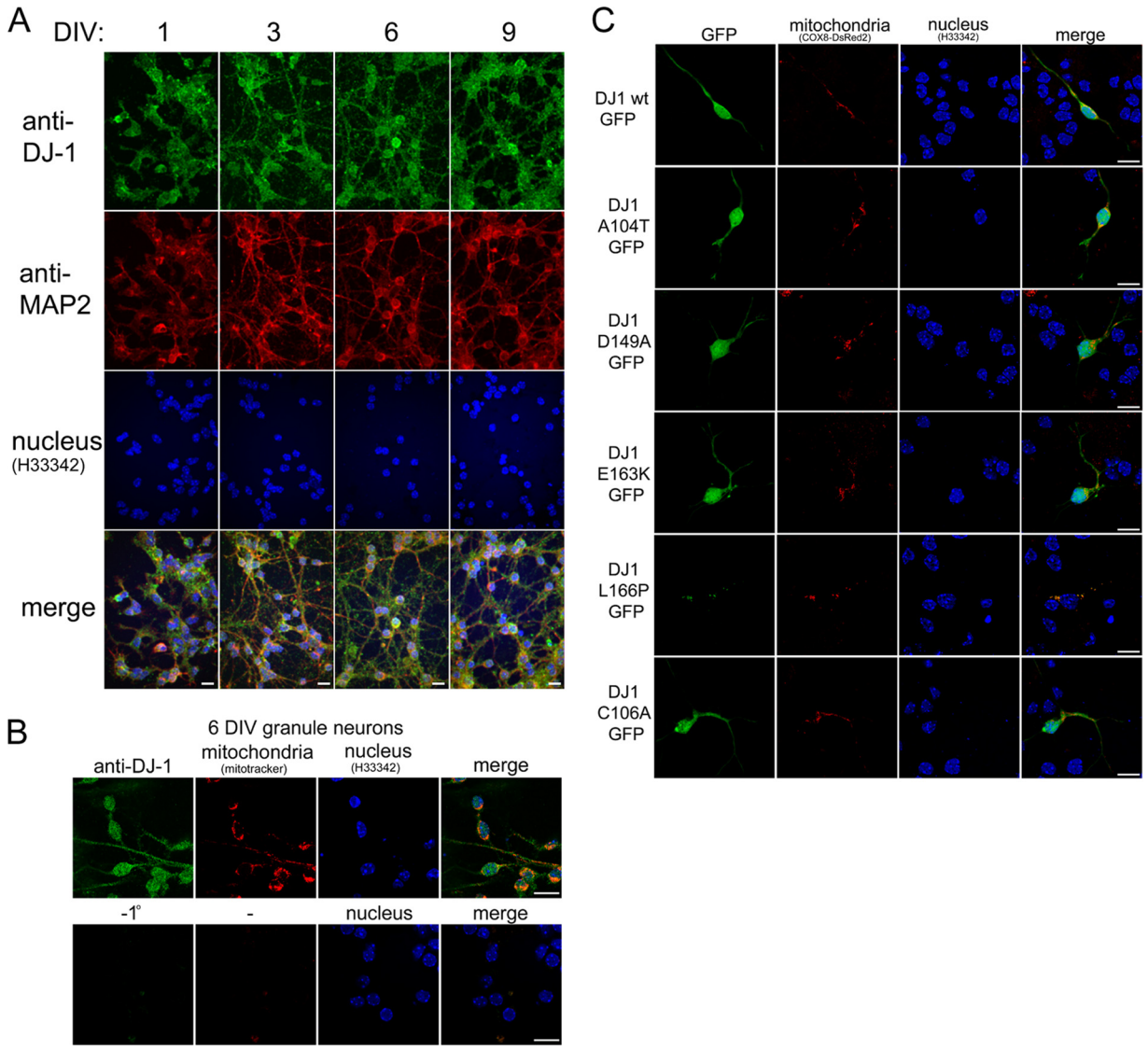

FIG 2 DJ-1 localization is not dependent on neuronal developmental stage. (A) CLSM images of developing 1 to 9 DIV primary granule neurons immunocytochemically stained for DJ-1 (green), MAP2 (red), and cell nuclei (blue). Maximum intensity scans are shown. Bar, 20 μm. (B) CLSM images of 6 DIV primary granule neurons immunocytochemically stained for DJ-1 (green), mitochondria (red), and cell nuclei (blue). −1°, staining without primary DJ-1 antibody. Bar, 20 μm. (C) CLSM images of 7 DIV primary granule neurons transiently expressing human wt DJ-1–GFP or the indicated point mutant DJ-1–GFP variants (green) for 24 h. Neurons were cotransfected with the mitochondrion marker COX8-DsRed2 (red) and counterstained with a nucleus marker (blue). Bar, 20 μm.

Immunoprecipitation. Immunoprecipitation of endogenous DJ-1 was from human neuroblastoma cells and overexpressed human DJ-1–GFP from transfected MEF DJ-$1^{-/-}$ cells. Cells were washed twice in ice-cold PBS, scraped off in PBS (with protease inhibitors), and pelleted at 100 × *g* for 5 min at 4°C. Cell pellets were lysed in 10 volumes of IP lysis buffer (20 mM morpholinepropanesulfonic acid [pH 7.2], 150 mM NaCl, 10% [vol/vol] glycerol) with 1% (vol/vol) Triton X-100 and protease inhibitors. Cell solutions were homogenized through a 27-gauge needle, incubated on ice for 10 min, and precleared at 12,000 × *g* for 10 min at 4°C. The supernatant was diluted 1:1 with IP lysis buffer (0.1% Triton X-100). Two micrograms of anti-DJ-1 or anti-GFP antibodies was added per sample, and the mixture was incubated at RT for 1 h. Protein samples were transferred to new vials to avoid extraction of plastic-bound proteins and incubated for 1 h with prewashed protein A/G magnetic beads (Dynabeads). Beads were washed three times in 1-ml volumes with IP lysis buffer followed by a wash three times in 1-ml volumes of IP lysis buffer (500 mM NaCl, 0.1% Triton X-100). Proteins were eluted by nondenaturing extraction using 0.1 M glycine (pH 2.8) prior to Western blot analysis.

Circular dichroism spectroscopy. *Escherichia coli* BL21(DE3) cells transformed with His-tagged DJ-1 wt or DJ-1/E163K were induced with isopropyl-β-D-thiogalactopyranoside at a 0.4 mM final concentration. Cells were incubated for 4 h, resuspended in lysis buffer (50 mM Tris-HCl [pH 7.5], 100 mM NaCl), and lysed with lysozyme (1 mg/ml final concentration) followed by freeze-thawing. After sonication, insoluble material was removed by pelleting at 20,000 rpm for 60 min at 4°C. Cleared lysates were loaded onto a Ni-nitrilotriacetic acid column (Qiagen), washed with 100 column volumes of 50 mM Tris-HCl (pH 7.5), 100 mM NaCl, 25 mM imidazole, and eluted with 5 volumes of 50 mM Tris-HCl (pH 7.5), 100 mM NaCl, 250 mM imidazole, and 10% (vol/vol) glycerol. DJ-1 wt and DJ-1/E163K proteins were buffer exchanged into 20 mM sodium phosphate buffer (pH 6.8) before analysis based on far-UV circular dichroism

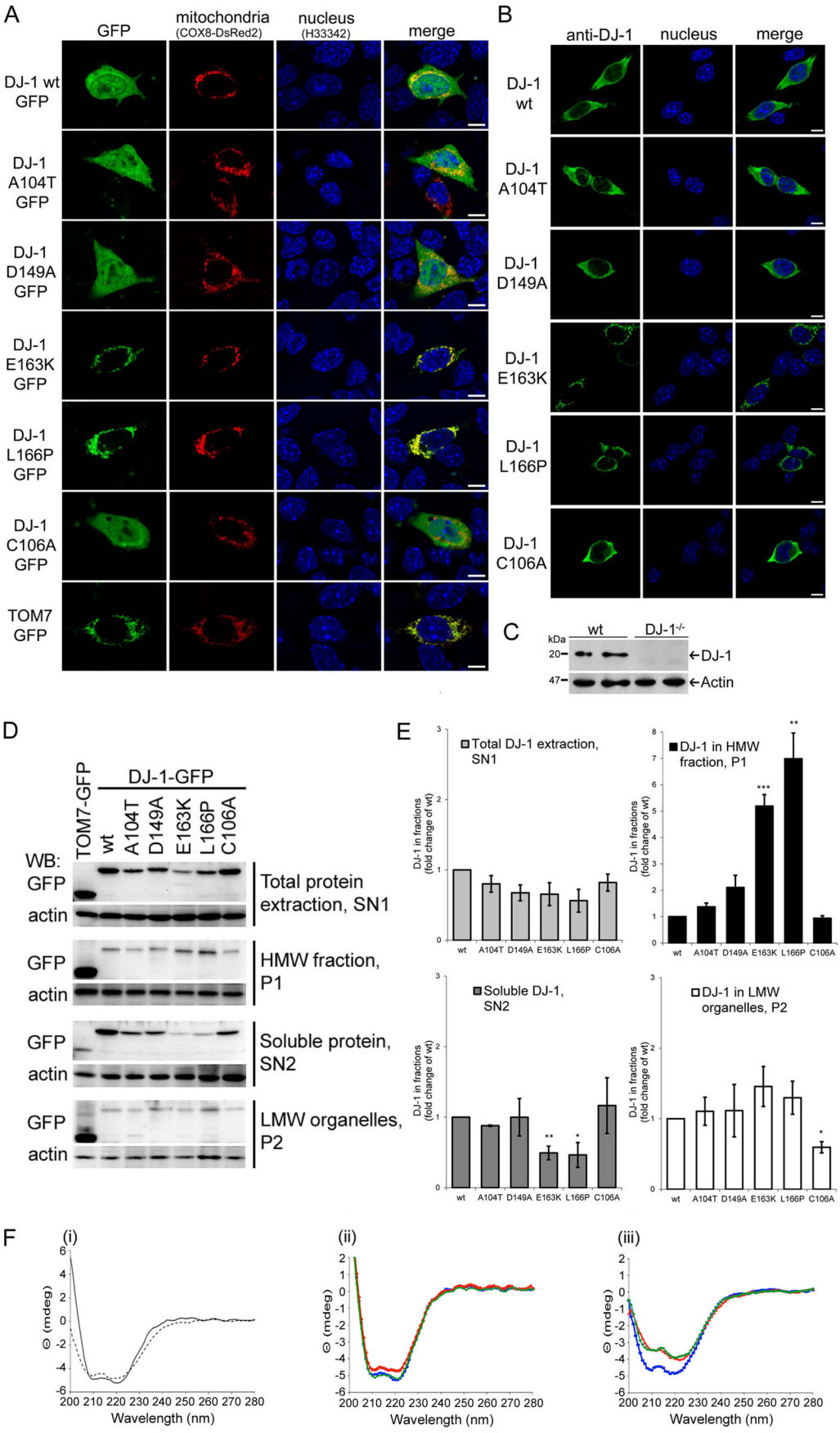
A
GFP
mitochondria (COX8-DsRed2)
nucleus (H33342)
merge
DJ-1 wt GFP
DJ-1 A104T GFP
DJ-1 D149A GFP
DJ-1 E163K GFP
DJ-1 L166P GFP
DJ-1 C106A GFP
TOM7 GFP
B
anti-DJ-1
nucleus
merge
DJ-1 wt
DJ-1 A104T
DJ-1 D149A
DJ-1 E163K
DJ-1 L166P
DJ-1 C106A
C
wt
DJ-1-/-
kDa
20
47
←DJ-1
←Actin
D
TOM7-GFP
DJ-1-GFP
wt
A104T
D149A
E163K
L166P
C106A
WB:
GFP
actin
Total protein extraction, SN1
HMW fraction, P1
Soluble protein, SN2
LMW organelles, P2
E
Total DJ-1 extraction, SN1
DJ-1 in HMW fraction, P1
Soluble DJ-1, SN2
DJ-1 in LMW organelles, P2
DJ-1 in fractions (fold change of wt)
wt A104T D149A E163K L166P C106A
F
(i)
(ii)
(iii)
Θ (mdeg)
Wavelength (nm)

(CD) spectra, which were recorded from 200 to 280 nm with 1-nm increments at 20°C and 37°C by using a Chirascan-plus CD spectrometer (Applied Photophysics).

Ethical approvals and use of laboratory animals. Collection of human postmortem brain tissue was approved by the Regional Committee for Medical and Health Research Ethics in western Norway. All research involving laboratory animals was approved by the National Animal Research Authority in Norway.

Statistical analysis. Statistical analysis was done using SPSS for Windows version 18.0 (SPSS, Chicago, IL). One-way analysis of variance followed by Fisher's least significant difference post hoc test was used for analysis of significance in samples with more than two variable groups. A Kruskal-Wallis test followed by Mann-Whitney U test was used for nonnormally distributed sample groups.

RESULTS

DJ-1 protein abundance is brain region specific and is regulated during neuronal development and neuritogenesis. We mapped DJ-1 protein levels in 25 major brain areas and brain nuclei in adult postmortem human brain. The whole brain from a donor without history of neurological disease was collected, and selected brain areas were harvested (39) and solubilized. Twenty micrograms of protein from each brain area was separated on an SDS-PAGE gel and analyzed quantitatively using antibodies for DJ-1 and for actin as a control (Fig. 1A). DJ-1 was expressed in all 25 human brain areas but showed up to 5-fold differences in levels between certain brain structures (Fig. 1A). The lowest levels were seen in areas originating from the brain stem. DJ-1 protein levels were increased in the striatum, hippocampal, and neocortical areas, with the highest levels in cerebellar areas. For comparison, we detected DJ-1 protein in major brain areas from postnatal day 6 mice (Fig. 1B).

We also characterized DJ-1 levels in our neuronal cell model system, the cerebellar granule neuron, during neuritogenesis at 1 to 9 DIV (Fig. 1C). The granule neurons can be obtained postnatally with high homogeneity and represent a useful model system due to due to their sustained physiological development in culture (40). DJ-1 protein levels increased during neuronal development *in vitro* and reached a significant 2-fold increase at 6 to 9 DIV (Fig. 1D). To assess if increased DJ-1 levels were due to developmental upregulation or prolonged culture conditions, we analyzed DJ-1 levels in brain tissue from mice at different developmental stages (postnatal days 1, 7, and 21 and in adults [6 months old]) (Fig. 1E). This experiment showed that DJ-1 levels are upregulated developmentally, as observed in both cerebellum and cerebral cortex. Our observations showed that DJ-1 abundance varies in a brain region-specific fashion and that DJ-1 increases during early neuronal development and neuritogenesis.

DJ-1 subcellular localization is not dependent on developmental stage. To determine if there is a change in subcellular localization patterns during neuritogenesis, we immunostained neurons at 1 to 9 DIV for DJ-1 and the neuron-specific cytoskeletal protein MAP2 (Fig. 2A). Despite the increase in DJ-1 expression at 6 to 9 DIV, there was no apparent change in localization in the developed neurons. Endogenously expressed DJ-1 had a predominantly soluble cytosolic localization in the neuronal cell body, neurites, and to a lower extent in the cell nuclei. A minimal preference for mitochondrial localization of endogenous DJ-1 was observed (Fig. 2B).

As various point mutant DJ-1 variants have been linked to neurodegeneration and early-onset PD, we generated GFP fusions to human wt DJ-1 and point mutant variants (A104T, D149A, E163K, L166P, and C106A). Transient expression of the GFP-tagged DJ-1 variants in neurons showed the same soluble, mainly cytosolic localization pattern as seen for endogenous DJ-1 (Fig. 2C). However, DJ-1/L166P-GFP showed mitochondrial localization (Fig. 2C), as first reported in COS-1 cells (41).

Mitochondrial localization of DJ-1/E163K is dependent on wt DJ-1 deficiency. DJ-1/L166P is easily degraded and does not form homodimers (42). To investigate the localization pattern of the DJ-1 variants in the absence of endogenous DJ-1, we used DJ-1 knockout MEF cells. Transient expression of wt DJ-1 or mutated DJ-1 variants in DJ-1$^{-/-}$ cells revealed a major difference between the cell types. Cytosolic DJ-1/E163K-GFP in neurons was exclusively localized to mitochondria in DJ-1$^{-/-}$ MEF cells (Fig. 3A). In DJ-1$^{-/-}$ cells, DJ-1/L166P localized as before to mitochondria, while wt DJ-1 and other variants (DJ-1/A104T, DJ-1/D149A, and DJ-1/C106A) remained cytosolic. Mitochondrial localization was confirmed using by the TOM7 signaling sequence fused to GFP and COX8-dsRed2. To confirm that GFP did not cause mislocalization, tagless DJ-1 variants were expressed in DJ-1$^{-/-}$ MEF cells and stained with an anti-DJ-1 antibody (Fig. 3B). The same mitochondrial localization pattern for tagless DJ-1/E163K and DJ-1/L166P was observed. Reduced nuclear localization of tagless DJ-1 wt and mutated DJ-1/A104T, DJ-1/D149A, and DJ-1/C106A was observed in comparison to GFP-tagged DJ-1, under nonstressed conditions. The absence of endogenous DJ-1 in DJ-1$^{-/-}$ cells was verified by Western blotting (Fig. 3C).

To verify the localization patterns for wt DJ-1 and the DJ-1 variants, we performed subcellular fractionation studies on trans-

FIG 3 DJ-1/E163K mitochondrial localization occurs in the absence of wt DJ-1. (A) CLSM images of MEF DJ-1$^{-/-}$ cells transiently expressing human wt DJ-1-GFP indicated point mutant DJ-1–GFP variants or the mitochondrion marker TOM7-GFP (green) for 24 h. Cells were cotransfected with the mitochondrion marker COX8-DsRed2 (red) and counterstained with a nucleus marker (blue). Bar, 10 μm. (B) CLSM images of MEF DJ-1$^{-/-}$ cells transiently expressing tagless human wt DJ-1 or point mutant DJ-1 variants for 24 h and immunocytochemically stained for DJ-1 (green) and a nucleus marker (blue). Single confocal scans though the cell nuclei are shown in both panels A and B. Bar, 10 μm. (C) SDS-PAGE and Western blot analysis of endogenous DJ-1 and actin protein expression in total cell lysates from wt and DJ-1$^{-/-}$ MEF cells. Results for two parallel samples are shown. (D) SDS-PAGE and Western blot analysis of GFP and actin protein expression in isolated cell fractions from DJ-1$^{-/-}$ cells transiently expressing human wt DJ-1–GFP, point mutant DJ-1–GFP variants, or the mitochondrion marker TOM7-GFP. SN1, total amount of extracted proteins including fractions P1, SN2, and P2 and excluding intact cells, nuclei, and cell debris; P1, high-molecular-weight (HMW) fraction containing large mitochondria; SN2, soluble proteins; P2, low-molecular-weight (LMW) fraction containing proteins bound to small organelles (lysosomes, peroxisomes, small mitochondria). (E) Quantification of data from images shown in panel A. All values were normalized to total protein extraction (SN1) and are shown as the fold change compared to wt DJ-1–GFP. The means ± standard errors of the means for three data sets are shown. *, $P < 0.05$; **, $P < 0.01$; ***, $P < 0.001$. (F) Irreversible loss of the alpha-helical secondary structure at physiological temperatures, based on the following analyses: (i) far-UV CD spectra of purified DJ-1 wt (solid line) and DJ-1/E163K (dashed line), recorded at 20°C; (ii) the DJ-1 wt spectrum (blue line) at 20°C, for the same sample after incubation at 37°C for 20 min (red line), and as rerecorded after equilibration at 20°C for 5 min (green line); (iii) the DJ-1/E163K spectrum (blue line) at 20°C, the same sample after incubation at 37°C for 20 min (red line), and as rerecorded after equilibration at 20°C for 5 min (green line).

fected DJ-1$^{-/-}$ MEF cells (Fig. 3D). Due to reduced stability of mutated DJ-1 (7, 42), especially DJ-1/L166P and DJ-1/163K, all values were normalized to total DJ-1 extraction (SN1) and are reported here as the fold change compared to wt DJ-1–GFP. A statistically significant increase in DJ-1/E163K and DJ-1/L166P was found in the high-molecular-weight organelle fractions containing mitochondria (Fig. 3E). DJ-1 wt, DJ-1/A104T, DJ-1/D149A, and DJ-1/C106 were predominantly found in the cytosolic fraction, while DJ-1/E163K and DJ-1/L166P were significantly reduced (Fig. 3D and E).

To test whether the E163K mutation had an effect on the overall structural integrity of DJ-1, we purified wt DJ-1 and DJ-1/E163K, followed by analysis using far-UV CD spectroscopy. We observed that DJ-1/E163K exhibited irreversible loss of the alpha-helical secondary structure at 37°C compared to the wt; this would possibly contribute to mitochondrial localization (Fig. 3F).

DJ-1/E163K is sequestered by wt DJ-1 in the cytosol through H_2O_2-dependent dimerization. Our analysis of DJ-1 localization in primary neuronal cultures and in DJ-1$^{-/-}$ cells demonstrated considerable localization differences for DJ-1/E163K (Fig. 2C and 3A). Since the lack of endogenous DJ-1 in DJ-1$^{-/-}$ cells was the most obvious difference, we hypothesized that wt DJ-1 was able to sequester DJ-1/E163K in the cytosol. To test this, we transiently coexpressed mutated variants of DJ-1–GFP with tagless wt DJ-1 in DJ-1$^{-/-}$ cells. Immunoprecipitation of GFP-tagged protein revealed that DJ-1/L166P was unable to heterodimerize with wt DJ-1, while DJ-1/E163K formed heterodimers with wt DJ-1 (Fig. 4A, left panel).

To analyze whether the DJ-1 variants could homodimerize, we transiently coexpressed wt DJ-1-GFP or DJ-1 variants fused to GFP with the corresponding DJ-1 mutant lacking GFP. Immunoprecipitation of GFP-tagged protein revealed that both DJ-1/E163K and DJ-1/L166P were unable to homodimerize (Fig. 4A, right panel). It is likely that the loss of DJ-1/E163K homodimerization is due to the loss of secondary structure (Fig. 3F).

To study the H_2O_2-induced stress protective mechanism of DJ-1, we initially assessed cell survival for DJ-1$^{-/-}$ cells and primary neurons exposed to increasing H_2O_2 concentration for 24 h (Fig. 4B and C). To further explore the H_2O_2 stress-induced mechanism of DJ-1 and its role in DJ-1 dimerization, we immunoprecipitated GFP-tagged DJ-1 variants from cells coexpressing tagless wt DJ-1 exposed to a nontoxic H_2O_2 concentration (30 μM) for 18 h. This revealed a clear reduction of coimmunoprecipitated tagless wt DJ-1, indicating that the DJ-1 dimers dissociated upon stress treatment (Fig. 4D). We then performed a time course experiment where we immunoprecipitated DJ-1–GFP after 0, 0.5, 2, 6, and 18 h of exposure to 30 μM H_2O_2 (Fig. 4E and F). Quantification of coimmunoprecipitated DJ-1 showed a significant loss of the DJ-1 dimer already after 2 h of exposure to H_2O_2. The wt DJ-1 homodimers and heterodimers of DJ-1/E163K–GFP and wt DJ-1 were equally affected.

To connect the above findings and to verify the observed molecular mechanism for DJ-1, we coexpressed red fluorescently tagged wt DJ-1 with DJ-1/E163K-GFP in DJ-1$^{-/-}$ cells and analyzed protein localization under control conditions and after 18 h of exposure to 30 μM H_2O_2 (Fig. 5A). In agreement with our previous findings, DJ-1/E163K–GFP exhibited cytosolic localization in the presence of wt DJ-1 under control conditions (Fig. 5A, upper panel). A clear segregation of mutated and wt DJ-1 was observed after H_2O_2 treatment, and translocation of DJ-1/E163K–GFP to mitochondria was observed (Fig. 5A, lower panel), confirming our initial findings. To confirm that the observed effect was independent of the fusion tag, we also coexpressed tagless wt DJ-1 with DJ-1/E163K–GFP and performed the stress treatment described above. The same soluble localization patterns with tagless wt DJ-1 under control conditions and segregation upon H_2O_2-induced stress were observed for DJ-1/E163K–GFP (Fig. 5B). Equal DJ-1 protein expression was confirmed by Western blotting (Fig. 5C).

We also assessed the loss of DJ-1 heterodimers upon treatment of primary neurons. The localization of transiently expressed DJ-1/E163K–GFP was analyzed under control conditions and after exposure to 30 μM H_2O_2 (Fig. 5D). DJ-1/E163K–GFP exhibited cytosolic localization under control conditions (Fig. 5D, upper panel, and 2C). However, a distinct translocation of DJ-1/E163K–GFP to mitochondria was observed in neurons exposed to H_2O_2 (Fig. 5D, lower panel).

DJ-1 translocates to the nucleus as a monomer in response to oxidative stress. We also observed via confocal laser scanning microscopy (CLSM) analysis an enhancement of wt DJ-1–GFP levels inside nuclei of transfected DJ-1$^{-/-}$ cells after exposure to 30 μM H_2O_2 for 24 h (Fig. 6A). By comparing the cross-sectional intensity profiles of DJ-1–GFP in control cells versus H_2O_2-treated cells, we measured a >60% increase in the mean fluorescence intensity (MFI) inside the cell nuclei (MFI_n) after H_2O_2 treatment (Fig. 6B). To further investigate the relocalization pattern of wt DJ-1 upon H_2O_2 treatment, we performed subcellular fractionation studies of wt DJ-1–GFP-expressing DJ-1$^{-/-}$ cells (Fig. 6C). Upon H_2O_2 treatment, a significant 2-fold increase in the total amount of wt DJ-1–GFP in the isolated cell nuclear fraction was observed (Fig. 6C and D). By using native polyacrylamide gel electrophoresis (native PAGE), we also confirmed that the increase in nuclear wt DJ-1–GFP was due to a significant accumulation of monomeric DJ-1 (Fig. 6C and D). No significant alterations of cytosolic wt DJ-1–GFP were observed upon H_2O_2 treatment (Fig. 6C and E).

Our findings showed that H_2O_2 treatment disrupts the DJ-1 dimeric complex and activates monomeric DJ-1 accumulation in the cell nuclei. To enable characterization of H_2O_2-activated monomeric DJ-1 in intact cells, we developed antibody S3618-2, which was devised to recognize only monomeric DJ-1. The antibody was designed to target amino acids 13 to 30, which comprise an exposed alpha-helical structure when DJ-1 is in its monomeric form, while this section of the protein is buried within the interface of the two DJ-1 protein monomers in the dimeric complex (Fig. 7A). The specificity of the newly produced DJ-1 antibody S3618-2 toward the synthetic peptide N′-GAEEMETVIPVDVMR RAG(C) was tested in an enzyme-linked immunosorbent assay (ELISA) (Fig. 7B and C). The specificity of anti-DJ-1 S3618-2 toward full-length DJ-1 was tested by immunocytochemical staining and Western blotting of wt and DJ-1$^{-/-}$ cells (Fig. 7D and E) To characterize the specificity of S3618-2 for monomeric DJ-1, wt DJ-1–GFP expressed in DJ-1$^{-/-}$ cells was separated by native PAGE and blotted with S3618-2 (Fig. 7F). The same membrane was reblotted with anti-GFP to identify both monomeric and dimeric forms of DJ-1–GFP (Fig. 7F). This characterization showed that S3618-2 has high specificity for the targeted peptide/protein and recognizes only the monomeric form of full-length DJ-1.

The localization pattern of endogenously expressed DJ-1 in primary neurons under control conditions or after exposure to 30

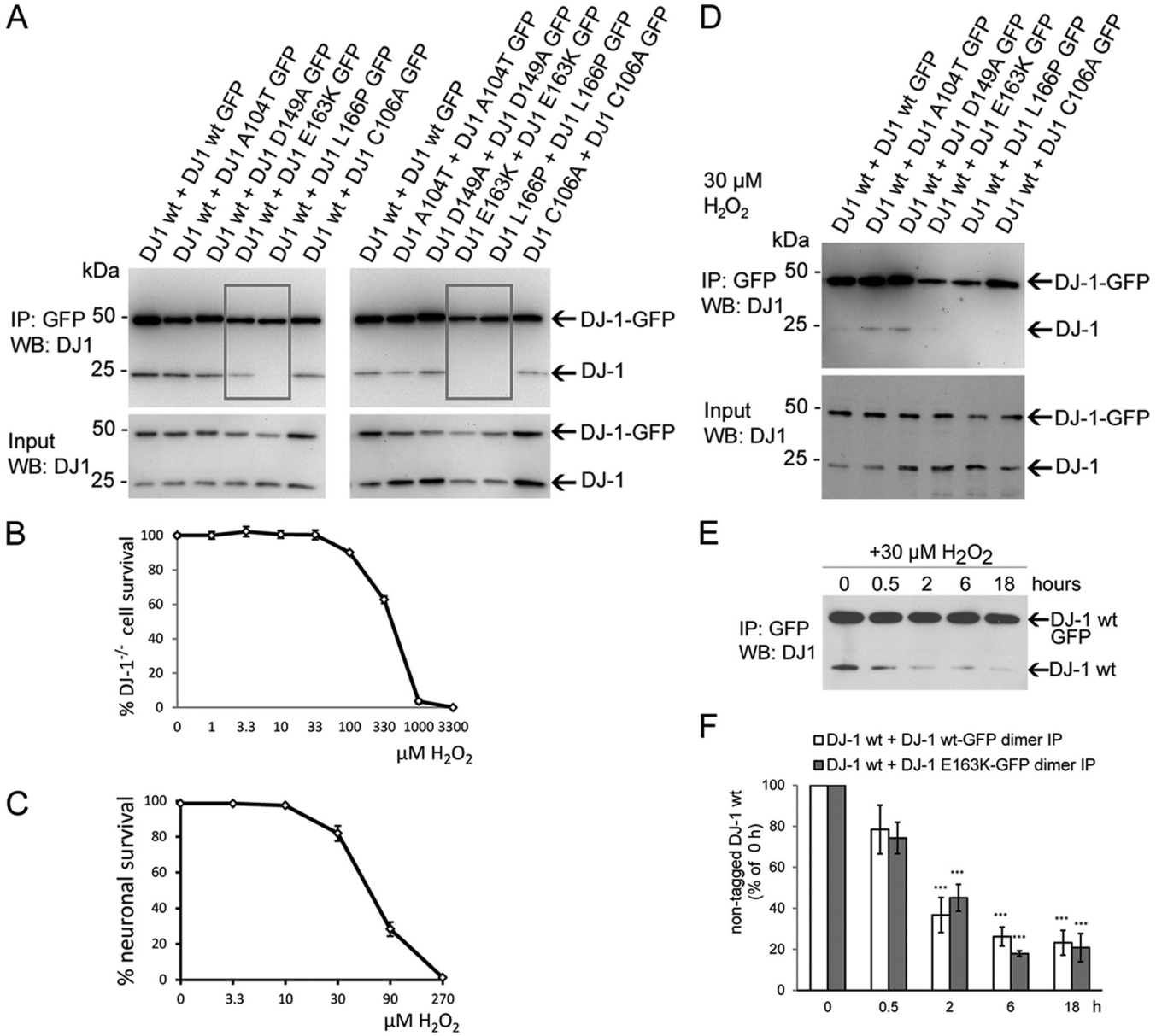

FIG 4 DJ-1/E163K is unable to form homodimers, and DJ-1 dimers are disrupted by H_2O_2-induced stress. (A, upper panel) SDS-PAGE and Western blot analysis of anti-GFP-immunoprecipitated human DJ-1 wt GFP or point mutant DJ-1–GFP variants expressed in DJ-$1^{-/-}$ cells coexpressing the indicated DJ-1 variant without a tag. Lack of coimmunoprecipitated DJ-1 is highlighted by the boxes. (Lower panel) Total cell lysate prior to immunoprecipitation. (B) Survival curve for MEF DJ-$1^{-/-}$ cells exposed to 0 to 3,300 μM H_2O_2 for 24 h. The means ± standard errors of the means (SEM) for five parallel data sets, repeated twice, are shown. (C) Survival curve for 6 DIV primary granule neurons exposed to 0 to 270 μM H_2O_2 for 24 h. The means ± SEM for four parallel data sets are shown. (D) SDS-PAGE and Western blot analysis of anti-GFP-immunoprecipitated human DJ-1-GFP variants, as shown in panel A, with the addition of 30 μM H_2O_2 stress for 18 h. (E) SDS-PAGE and Western blot analysis of anti-GFP-immunoprecipitated human wt DJ-1–GFP and coimmunoprecipitated tagless wt DJ-1 from DJ-$1^{-/-}$ cells exposed to 30 μM H_2O_2 stress for 0 to 18 h. (F) Quantification of results shown in panel E for coimmunoprecipitated tagless wt DJ-1 upon exposure to 30 μM H_2O_2 stress for 0 to 18 h E. Means ± SEM for three data sets are shown. All values are shown as a percentage of the 0-h control. ***, $P < 0.001$.

μM H_2O_2 for 18 h was further assessed by immunocytochemical staining (Fig. 8). Detection of total DJ-1 protein in intact neuron under control conditions showed the same predominantly cytosolic expression pattern (Fig. 8A, upper panel). Exposure to H_2O_2 and analysis of total DJ-1 by CLSM did not, by visual analysis, detect any dramatic change in total DJ-1 localization (Fig. 8A, lower panel). However, by comparing the cross-sectional intensity profiles of total DJ-1 protein (Fig. 8B), we measured a significant 2-fold increase in the nuclear MFI after H_2O_2 exposure (Fig. 8C). In parallel, the localization pattern of endogenous monomeric DJ-1 in primary neurons was assessed using S3618-2 (Fig. 8D to F). Under control conditions we observed nuclear localization for monomeric DJ-1, while dramatic enhancement of the nuclear monomeric DJ-1 signal was detected in the neurons after 30 μM H_2O_2 treatment (Fig. 8D). Cross-sectional intensity profiles of monomeric DJ-1 again confirmed a significant increase in the nuclear MFI after H_2O_2 treatment (Fig. 8E and F). We also detected reducted monomeric DJ-1 in the cytosol after H_2O_2 treat-

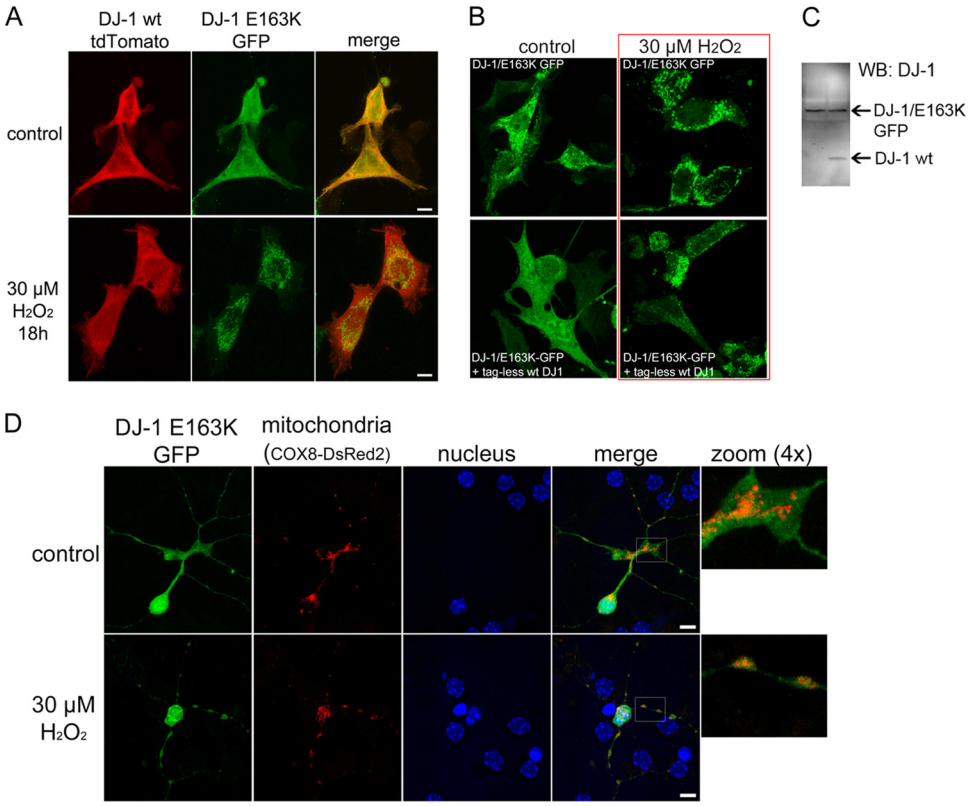

FIG 5 DJ-1 wt sequesters DJ-1/E163K in the cytosol through H_2O_2-dependent dimerization. (A) CLSM images of DJ-$1^{-/-}$ cells transiently expressing human wt DJ-1–pdtTomato (red) and DJ-1/E163K–GFP (green), in the presence of absence of 30 μM H_2O_2 for 18 h. Bar, 10 μm. (B) CLSM images of MEF DJ-$1^{-/-}$ cells expressing DJ-1/E163K–GFP only (upper panel) or coexpressed with tagless wt DJ-1 (lower panel). DJ-1/E163K–GFP localized to mitochondria if wt DJ-1 was not present (upper panel). DJ-1/E163K–GFP stayed in the cytoplasm when coexpressed with wt DJ-1 (lower left panel), whereas mitochondrial relocalization of DJ-1/E163K–GFP was apparent after H_2O_2-induced stress for 18 h (lower right). (C) Anti-DJ-1 Western blot for protein expression for images shown in panel B. (D) CLSM images of wt 7 DIV primary granule neurons transiently expressing point mutants of human DJ-1/E163K–GFP (green) and the mitochondrial marker COX8-DsRed2 (red), in the absence or presence of 30 μM H_2O_2 for 24 h. Neurons were counterstained with a nuclear marker (blue). Bar, 10 μm.

ment, indicating that monomeric DJ-1 that formed in the cytosol was transported into the nuclei (Fig. 8F).

Nuclear translocation of monomeric DJ-1 is mediated by karyopherin β2 binding to the DJ-1 PY-NLS and is enhanced by oxidative stress. We found that human DJ-1 lacks classical NLSs (43). However, a nonclassical PY-NLS consensus sequence (44) was identified in human DJ-1 and found to be conserved between species (Fig. 9A). The PY-NLS sequence had an N-terminal hydrophobic motif and was localized within amino acids 50 to 67. To test whether this PY-NLS sequence could act as a DJ-1 nuclear localization driver, we constructed a set of GFP expression vectors containing N-terminal signaling peptides from human DJ-1 (Fig. 9B). By expressing the constructed fusions in DJ-$1^{-/-}$ cells, we could observe a pronounced localization of GFP to the cell nuclei in cases where the DJ-1 PY-NLS sequence was included in the N-terminal signaling peptide (Fig. 9C). None of the tested DJ-1 signaling peptides that were fused to GFP were seen to localize to mitochondria. The PY-NLS consensus sequence enables nuclear localization through a direct interaction with karyopherin β2 (44). To determine if human DJ-1 was able to bind to karyopherin β2, we immunoprecipitated endogenous DJ-1 from human neuroblastoma cells and analyzed the purified DJ-1 for coimmunoprecipitated karyopherin β2 (Fig. 9D). Our analysis showed that endogenously expressed karyopherin β2 coimmunoprecipitated with DJ-1 and that the binding could be enhanced more than 2-fold by exposing cells to 30 μM H_2O_2. To further test if DJ-1 binding to karyopherin β2 was affected by C106 oxidation state or PD mutation, we also immunoprecipitated GFP-tagged DJ-1 mutants. Endogenously expressed karyopherin β2 coimmunoprecipitated with DJ-1/C106A, DJ-1/A104T, and DJ-1/D149A, while coimmunoprecipitation with DJ-1/E163K was not detected (Fig. 9E). This analysis indicated that oxidation of C106 is not crucial for DJ-1 binding to karyopherin β2 and subsequent nuclear translocation. It also showed that DJ-1/E163K is not actively transported by karyopherin β2, which may have an implication for DJ-1/E163K mitochondrial delocalization.

DISCUSSION

In this study, we investigated the cytoplasm-mitochondrion and cytoplasm-nucleus trafficking of DJ-1 and its mutated variants. We demonstrated that translocation from the cytosol to either organelle is dependent on a shift from a dimeric to a monomeric state, which is determined by the oxidative environment and the nature of the mutated forms of DJ-1. Combined with our findings that DJ-1 abundance is brain region specific and that its levels are regulated during neuronal development and neuritogenesis, our data provide new insights into the developmental and intracellu-

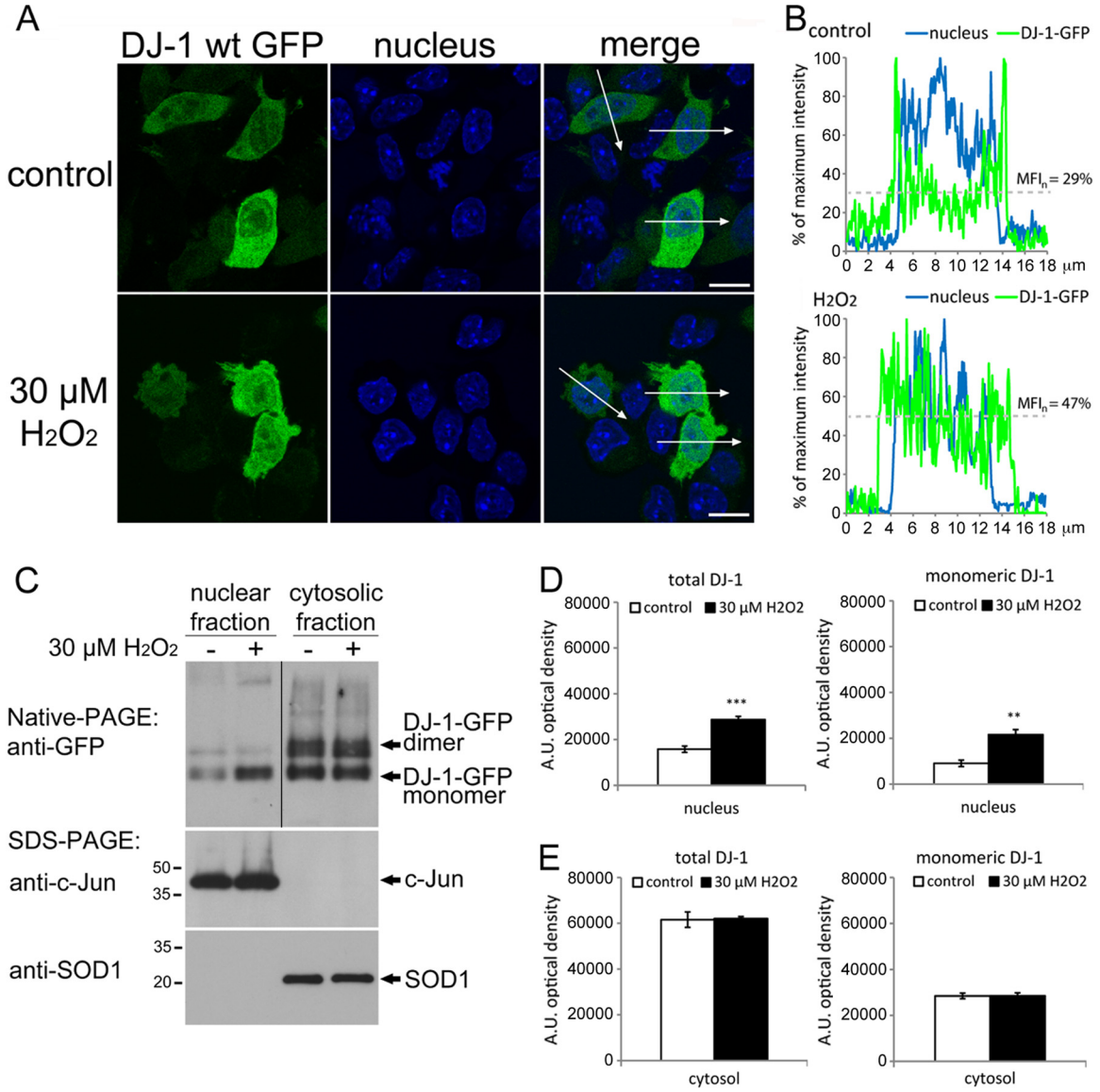

FIG 6 DJ-1 is observed in the nucleus as a monomer in response to oxidative stress. (A) CLSM images of DJ-1$^{-/-}$ cells transiently expressing human wt DJ-1-GFP (green), in the presence of absence of 30 μM H_2O_2 for 24 h, and counterstained with the nucleus marker Hoechst 33342 (blue). Cross-sectional areas are marked with arrows. Single confocal scans though the cell nuclei are shown. Bar, 10 μm. (B) Cross-sectional intensity profiles for the areas indicated with arrows in panel A. To enable sample comparisons, the background intensity was subtracted, and values were normalized as the percent maximum intensity for both wt DJ-1–GFP (green) and nuclear (blue) intensity profiles. Mean values for the six cross-sectional areas marked in panel A are shown. (C, upper panel) Native PAGE and Western blot analysis of DJ-GFP expression in isolated cell fractions from DJ-1$^{-/-}$ cells transiently transfected with human wt DJ-1–GFP, in the presence of absence of 30 μM H_2O_2 for 24 h. (Middle and lower panels) SDS-PAGE and Western blot analysis of the nuclear transcription factor c-Jun and cytoplasmic SOD1 in isolated cell fractions from transfected DJ-1$^{-/-}$ cells. (D) Quantification of expressed wt DJ-1–GFP in the isolated nuclear cell fractions, in the presence or absence of 30 μM H_2O_2 for 24 h, shown in panel C. Means ± standard errors of the means (SEM) for three data sets are shown. **, $P < 0.01$; ***, $P < 0.001$. (E) Quantification of expressed wt DJ-1–GFP in the isolated cytosolic cell fractions, in the presence or absence of 30 μM H_2O_2 for 24 h, shown in panel C. Means ± SEM for three data sets are shown.

lar dynamic nature of DJ-1, which possibly contributes to its observed pleiotropic nature.

Within neurons, DJ-1 appears to be critical as a neuroprotectant, as seen in response to oxidative stress, and in maintaining mitochondrial integrity (9–13). As alterations in neuronal function in PD subjects is widespread and is observed in a predominant caudal-to-rostral progression, it is reasonable to expect that PD-associated genes may be differentially regulated within different brain regions. Indeed, *DJ-1* mRNA levels vary depending on the brain region (45). We have extended this analysis by analyzing DJ-1 protein levels in 25 different human brain regions. We found a low abundance of DJ-1 in areas originating from the brain stem, while elevated DJ-1 levels were found in the striatum, hippocampal, neocortical, and cerebellar areas (Fig. 1A). This brain region-specific DJ-1 abundance pattern indicates that the need for DJ-1-mediated neuroprotection may vary within different brain substructures. This may also be the case during neuronal development and neuritogenesis, as DJ-1 protein levels increase during

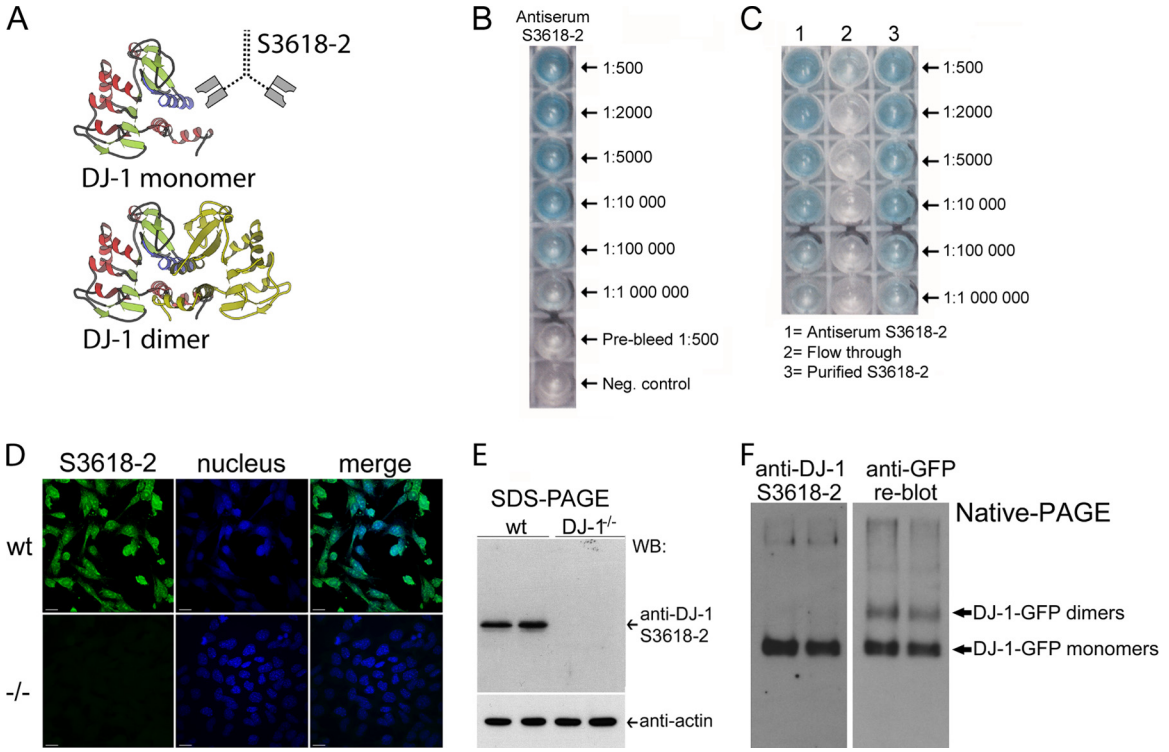

FIG 7 Characterization of antibody S3618-2, which targets monomeric DJ-1. (A) Crystal structure models of human DJ-1 in its monomeric and dimeric forms. The antibody S3618-2, which targets alpha-helical DJ-1 domain 13-30, is highlighted in blue. The protein structure was adopted from PDB ID 2R1V. (B) ELISA analysis results of antiserum for antibody S3618-2 against immunizing peptide N′-GAEEMETVIPVDVMRRAG(C); the antibody targets DJ-1 amino acids 13 to 30. Prebleed serum at the highest concentration (1:500 dilution) was used as the reference. (C) ELISA analysis results for purified S3618-2 antibody against immunizing peptide. (D) Immunocytochemical staining of wt and DJ-$1^{-/-}$ MEF cells, using anti-DJ-1 S3618-2 antibody (green) and Hoechst 33342 (blue) nuclear stain. Bar, 10 μm. (E) Denaturing SDS-PAGE and Western blot results for total cell lysates from wt and DJ-$1^{-/-}$ MEF cells. Membranes were probed with antibody anti-DJ-1 S3618-2; an antiactin was used as the loading control. (F) Native PAGE and Western blot analysis of DJ-GFP expressed in DJ-$1^{-/-}$ cells transiently transfected with human wt DJ-1–GFP. (Left) Membrane blotted with anti-DJ-1 S3618-2 antibody, which recognizes monomeric DJ-1. (Right) The same membrane, reblotted with anti-GFP, which recognized the GFP tag on both monomeric and dimeric DJ-1–GFP. Full-length blots of two parallel samples are shown.

early neuronal development *in vitro* (Fig. 1D) and during brain development in mice *in vivo* (Fig. 1E).

DJ-1 represents a dynamic protein (7, 16, 17). It appears that the cytosol represents the default localization of homodimeric wt DJ-1 under nonstressed conditions (7, 20, 46). In response to oxidative damage, wt DJ-1 does show mitochondrial accumulation that is dependent on Parkin and possibly PINK1 (46). The first identified pathogenic PD DJ-1 mutant, DJ-1/L166P, which is unable to form homodimers, translocates to mitochondria (4, 31, 47). DJ-1/L166P also exhibits reduced stability and enhanced proteasome-mediated degradation, which possibly contribute to the altered localization patterns (31). Mitochondrial localization is also mediated by C106 oxidation (7) but is not essential, as DJ-1/E18A lacking C106 oxidation also translocates to mitochondria (20). We showed that DJ-1/E163K forms heterodimers with wt DJ-1 and that wt DJ-1 retains DJ-1/E163K in the cytosol under nonoxidative conditions (Fig. 1O). However, DJ-1/E163K is unable to homodimerize and translocates to mitochondria in the absence of wt DJ-1, as is also the case for DJ-1/L166P (Fig. 3A). DJ-1/L166P is unable to interact with wt DJ-1, suggesting that DJ-1/E163K represents a unique variant in terms of its homo- and heterodimeric potential (Fig. 3). Interestingly, DJ-1/A104T, DJ-1/D149A, and DJ-1/C106A were able to form homodimers and heterodimers with wt DJ-1 (Fig. 3A and 4A). Although it has been shown that DJ-1/A104T and DJ-1/E163K remain unchanged in terms of their secondary structure and dimerization potential at 20°C (48), we showed that DJ-1/E163K irreversibly looses alpha-helical secondary structures at physiological temperatures, possibly explaining the loss of dimerization and mitochondrial translocation (Fig. 3F). *In vitro* studies, using differential scanning calorimetry, have indeed shown that the E163K mutation decreases the thermal stability of the homodimer by at least 11°C (48). This is mainly the result of disruption of the salt bridge formed with R145 of the corresponding monomer. We note that this interaction is likely a strongly conserved feature, as evidenced by the highly conserved nature of these positions in DJ-1 homologs. The heterodimer would conserve one half of the salt bridge interaction and may in fact explain how the heterodimer influences the stability of the E163K mutant.

The DJ-1 peroxiredoxin-like peroxidase activity and its H_2O_2-scavenging ability (6) suggest that oxidative stress influences its localization dynamics. Both wt DJ-1 and DJ-1/C106A translocate to mitochondria in response to oxidative stress (4, 7, 46), and DJ-1/L166P and DJ-1/M26I, which do not homodimerize, are mitochondrial variants (4, 20, 49). We showed here that the heterodimerization abilities of DJ-1/A104T, DJ-1/D149A, and DJ-1/C106A with wt DJ-1 are either absent (C106A) or highly reduced (A104T and D149A) in the presence of nontoxic H_2O_2 levels

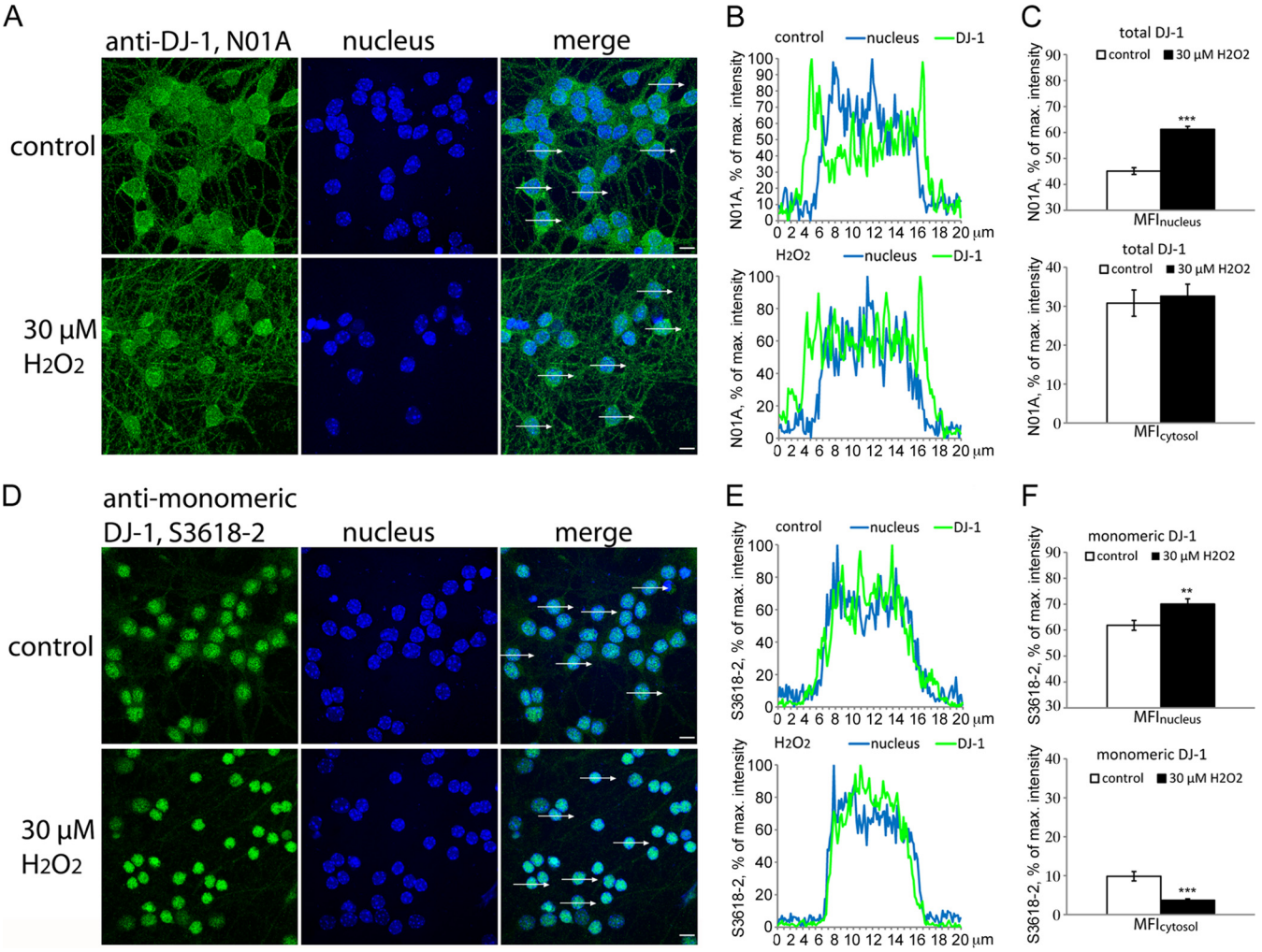

FIG 8 Oxidative stress induces the translocation of monomeric DJ-1 from the cytosol to the nucleus in primary neurons. (A) CLSM images of 7 DIV primary neurons, with or without treatment with 30 μM H_2O_2 for 18 h and immunocytochemically stained with pan-anti-DJ-1 N01A (green) for detection of the total amount of endogenously expressed DJ-1. Neurons were counterstained with the nucleus marker Hoechst 33342 (blue). Cross-sectional areas are marked with arrows. Bar, 10 μm. (B) Cross-sectional intensity profiles for the areas indicated by arrows in panel A. To enable sample comparisons, the background fluorescence was subtracted, and values were normalized as the percent maximum intensity for both anti-DJ-1 N01A (green) and nuclear (blue) intensity profiles. Mean values for the 12 cross-sectional areas marked in panel A are shown. (C) Quantification of total DJ-1 MFI in the nucleus (top) and in the cytosol (bottom) of primary neurons, with or without exposure to 30 μM H_2O_2 for 18 h, shown in panel B. The mean ± standard error of the mean (SEM) intensity is shown. ***, $P < 0.001$. (D) Results for the same experimental setup as shown in panel A, with the exception that endogenously expressed neuronal DJ-1 was detected with anti-DJ-1 S3618-2 antibody, which recognizes monomeric DJ-1. Single confocal scans though the cell nuclei are shown in both panels A and D. Bar, 10 μm. (E) Cross-sectional intensity profiles for the areas indicated with arrows in panel D. The experimental setup was the same as that described for panel B. Mean values for the 12 cross-sectional areas marked in panel D are shown. (F) Quantification of monomeric DJ-1 MFI in the nucleus (top) and in the cytosol (bottom) of primary neurons, with or without exposure to 30 μM H_2O_2 for 18 h, shown in panel E. The mean (±SEM) intensities are shown. **, $P < 0.01$; ***, $P < 0.001$.

(Fig. 4D). However, we did not observe any mitochondrial recruitment of DJ-1/A104 or DJ-1/D149 in the absence of or in response to H_2O_2, Paraquat, metals (Cu, Co, Fe), dopamine, or DOPAL treatments (data not shown) demonstrated that mitochondrial localization mediated through dimerization is mutation dependent. We also showed that wt DJ-1 loses it homodimerization ability in response to H_2O_2 exposure and that this is time dependent: homodimerization is almost completely abolished after 2 h of oxidative stress treatment (Fig. 4E). Indeed, the heterodimerization of wt DJ-1 with DJ-1/E163K was equally affected (Fig. 4F). A recent study showed that paraquat or H_2O_2 exposure of HEK 293T cells overexpressing wt DJ-1 bimolecular fluorescent complementation (BiFC) constructs led to an enhancement of the fluorescence BiFC signal, suggesting oxidative stress-mediated stabilization of wt DJ-1 homodimers (50). The ambiguity of the expermental data may be due to BiFC technology disadvantages, as formation of the fluorescent complex is irreversible, making it challenging to detect dimerization loss (51). It is therefore essential to verify BiFC-positive interactions by a separate approach. To this end, we showed that DJ-1/E163K remains cytosolic under nonstressed conditions, while a clear translocation to mitochondria occurred in response to H_2O_2 treatment both in DJ-$1^{-/-}$ MEF cells coexpressing wt DJ-1 and DJ-1/E163K and in primary wt neurons expressing DJ-1/E163K (Fig. 5A to D). Combined, these data demonstrate that DJ-1 cytoplasm-mitochondrion trafficking is dependent on (i) the dimerization state of

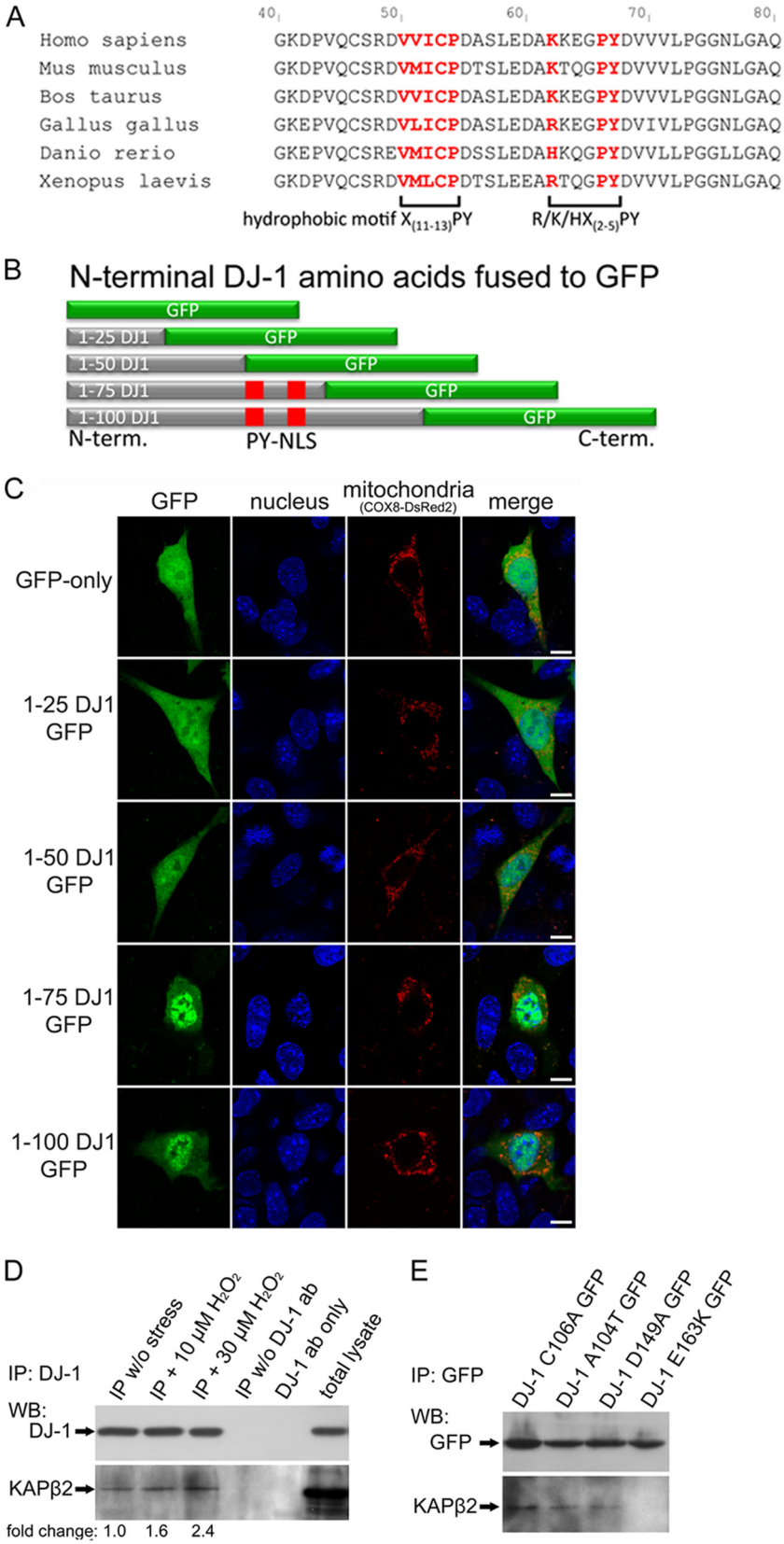

FIG 9 Karyopherin β2 interacts with DJ-1 PY-NLS in an oxidative stress-dependent manner, leading to nuclear translocation of monomeric DJ-1 from the cytosol. (A) Amino acid sequence alignment of DJ-1 from the indicated species. The conserved PY-NLS consensus sequence (hydrophobic motif, $X_{(11–13)}$ PY, R/K/H$X_{(2–5)}$PY) was identified at location 50 to 67 in human DJ-1 (highlighted in red). (B) Schematic illustration of the constructed N-terminal DJ-1 signaling

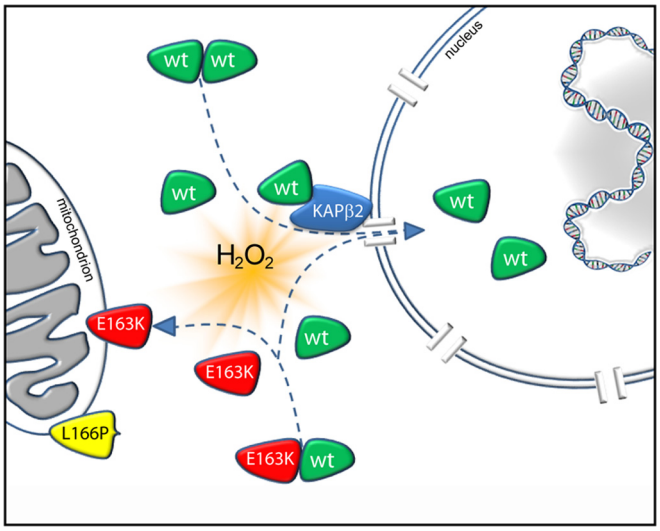

FIG 10 Model for oxidative stress-dependent cytoplasm-mitochondrion and cytoplasm-nucleus DJ-1 trafficking in neuronal cells. Under normal conditions, DJ-1 is present as a dimeric cytosolic structure. Upon oxidative stress, activation of DJ-1 dimerization is disrupted, followed by an interaction, through its PY-NLS domain, with karyopherin β2 (KAPβ2), which translocates cytosolic monomeric DJ-1 to the nucleus. The clinical DJ-1 mutation E163K has a profound effect on cytoplasm-mitochondrion trafficking in neurons. Under normal physiological conditions, wt DJ-1 is able to sequester DJ-1/E163K in the cytosol. However, in response to oxidative stress, this dimerization is disrupted, leading to DJ-1/E163K translocation to mitochondria. As DJ-1/E163K is unable to form homodimeric structures, a homozygous DJ-1/E163K state leads to the accumulation of an antioxidant-defective DJ-1.

both wt DJ-1 and mutant variants, (ii) the hetero- or homozygotic nature of the DJ-1/E163K allele, and (iii) the cellular oxidative environment (Fig. 10). The protective role of DJ-1 toward mitochondria can be explained in part by its direct H_2O_2-scavenging ability (6). The protective mitochondrial role of DJ-1 may also align with the roles of Parkin and PINK1. PINK1 and Parkin maintain mitochondrial integrity, and DJ-1 forms a complex with PINK1 and Parkin that promotes ubiquitination of Parkin substrates (52). However, genetic studies have revealed that DJ-1 can rescue PINK1 but not Parkin loss-of-function phenotypes, that Parkin and PINK1 are unable to rescue DJ-1 loss-of-function phenotypes, and that PINK1-mediated mitochondrial fragmentation cannot be rescued by DJ-1 (53). Studies have also shown that DJ-1 is recruited to mitochondria in response to oxidative stress and that this is dependent on Parkin and possibly PINK1 (46). Clearly, the interplay between these three proteins is complex, but the possibility exists that their molecular relationship is influenced by the degree of oxidative stress, combined with specific DJ-1 mutations.

DJ-1/E163K results in a severe phenotype that includes Parkinsonism, cognitive decline, and amyotrophic lateral sclerosis at an early age (25 years) when subjects are homozygous for the mutation (54). In line with this, we found that DJ-1/E163K, in the presence of wt DJ-1 (heterozygous state), was retained in the cytosol while mitochondrial translocation of DJ-1/E163K occurred in the absence of wt DJ-1 (homozygous state). DJ-1/E163K does not rescue cells under conditions of oxidative stress, and it is possible that DJ-1/E163K homozygous subjects harbor neurons that are vulnerable to oxidative stress due to the mitochondrial translocation of antioxidant-deficient DJ-1/E163K. Conversely, in a heterozygous state, the wt DJ-1 retains DJ-1/E163K in the cytosol through heterodimerization, perhaps allowing a fraction of wt DJ-1 monomers, released from the homodimeric state, to translocate to mitochondria in response to oxidative stress. However, the plausibility of this may depend on the stability of DJ-1/E163K, as both wt DJ-1 homodimers and wt DJ-1/DJ-1/E163K heterodimers showed a similar reduction in dimerization potential in response to oxidative stress (Fig. 4F).

Within the nucleus, DJ-1 has several roles. DJ-1 can interact with and sequester Daxx, leading to loss of Ask1 activation and prevention of cell death (55, 56). DJ-1 also acts as a coactivator of various pathways, including that for the androgen receptor (24, 25), Nrf2-mediated detoxification (26), and the p53 pathway (27, 28). DJ-1 has been shown to be a neuroprotective transcriptional coactivator that binds to PSF and also to the TH promoter, ultimately regulating dopamine production (29, 30). Although DJ-1 can be redirected to the nucleus, the mechanisms are unknown. DJ-1 can translocate into the nucleus under normal conditions, and we showed that nuclei of cells exposed to nontoxic levels of H_2O_2 had a 2-fold increase in total nuclear accumulation of DJ-1–GFP (Fig. 6A and B). This was in agreement with recent studies that showed DJ-1 nuclear localization in response to both 6-hydroxydopamine and H_2O_2 treatment (57). Based on our findings that oxidative stress disrupts DJ-1 dimerization and that DJ-1 monomers translocate to mitochondria, we also found that the increase in oxidative stress-mediated nuclear DJ-1–GFP levels was due to accumulation of the monomeric form of DJ-1 (Fig. 6C and D). This demonstrated that relocation of DJ-1 from its default cytosolic localization to either mitochondria or the nucleus depends on the oxidative environment and the conversion from a dimeric to a monomeric state (Fig. 10).

We generated a unique monomeric form-specific anti-DJ-1 antibody (Fig. 7) to characterize endogenous monomeric DJ-1 nuclear accumulation *in vivo*. We found that endogenous DJ-1 in primary neurons translocates to the nucleus in response to oxidative stress (Fig. 8A to C), verifying that nuclear translocation is due to DJ-1 and not the GFP fusion partner or to overexpression. Although DJ-1–GFP accumulates in nuclei as a monomer in response to oxidative stress (Fig. 6), DJ-1 monomeric structures may be imported into the nucleus either as a monomer or as a dimer that undergoes a state change within the nucleus. We found a significant increase in nuclear monomeric DJ-1 in response to

peptides fused to full-length GFP. The two domains of the identified PY-NLS sequence, spanning amino acids 50 to 67, are highlighted in red. The length of the illustrated signaling peptides and full-length GFP are not in proportion to their actual sizes. (C) CLSM images of DJ-$1^{-/-}$ cells transiently expressing N-terminal DJ-1 signaling peptides fused to full-length GFP (green), as illustrated in panel B. Cells were cotransfected with the mitochondrion marker COX8-DsRed2 (red) and counterstained with a nucleus marker (blue). Bar, 10 μm. (D) SDS-PAGE and Western blot analysis of immunoprecipitated (IP) endogenously expressed DJ-1 and coimmunoprecipitated endogenously expressed karyopherin β2 from human neuroblastoma cells. The cells were exposed to 0 to 30 μM H_2O_2 for 18 h prior to immunoprecipitation. The change in coimmunoprecipitated karyopherin β2 upon H_2O_2-induced stress is indicated as the fold change compared to cells without stress. (E) SDS-PAGE and Western blot analysis of immunoprecipitated overexpressed mutated DJ-1–GFP variants and coimmunoprecipitated endogenously expressed karyopherin β2 from human neuroblastoma cells.

oxidative stress, with an associated decrease in cytosolic monomeric DJ-1 (Fig. 8D to F), suggesting that endogenous DJ-1 is translocated to the neuronal nucleus as a monomer (Fig. 10).

DJ-1 lacks a classical NLS but contains a nonclassical PY-NLS sequence at the N terminus (amino acids 50 to 67), which shows a high degree of conservation (Fig. 9A). The ability of this PY-NLS sequence to specifically translocate wt DJ-1 into the nucleus was shown by working with PY-NLS-GFP fusions (Fig. 9B), in which nuclear localization was observed when the PY-NLS was present in the targeting sequences (Fig. 9C). Karyopherin β2 can interact directly with PY-NLS sequences, mediating nucleocytoplasmic trafficking, and we showed that wt DJ-1 interacts with karyopherin β2 (Fig. 9D). Interestingly, we found that a nontoxic H_2O_2 concentration enhanced the DJ-1 PY NLS–karyopherin β2 interaction more than 2-fold compared to control cells (Fig. 9D). Within the DJ-1 three-dimensional structure, we observed that the PY-NLS sequence (amino acids 50 to 54) is partly buried between the DJ-1 monomeric interfaces. This observation suggests that karyopherin β2 preferentially binds to monomeric DJ-1 with the entire PY-NLS sequence exposed. Combined, these results suggest that monomeric wt DJ-1 can bind to karyopherin β2 through its PY-NLS sequence, which leads to karyopherin β2-mediated nuclear translocation, and that this translocation is increased by oxidative stress (Fig. 10). Alanine substitution at the oxidation site C106 did not render DJ-1 able to bind to karyopherine β2 (Fig. 9E). This indicated that oxidation-induced monomerization, rather than specific C106 oxidation, is the driving force for DJ-1 nuclear translocation. We believe that a predominant part of the H_2O_2-activated monomeric wt DJ-1 remains in the cytosol by reforming homodimeric DJ-1 complexes, and this warrants further investigation.

The dynamic trafficking of cytosolic DJ-1 to mitochondria and the nucleus in response to oxidative stress and as seen with DJ-1 mutant variants overshadows its potential roles in the cytosol. However, the ability of DJ-1 to bind RNA targets in the cytosol in an oxidative stress-dependent manner (21) suggests that DJ-1 plays pivotal roles in all three subcellular locations, with oxidative stress being the common denominator.

ACKNOWLEDGMENTS

This work was supported by a grant from the Western Norway Regional Health Authority (Helse Vest project grant 911575).

We thank Lara Aqrawi for expert technical assistance. We thank Darren Moore (Brain Mind Institute, EPFL, Switzerland) for the rabbit monoclonal anti-DJ-1 antibody (N01A), Huaibin Cai (National Institute on Aging, NIH, Bethesda, MD) for DJ-1$^{-/-}$ MEF cells, Michael J. Courtney (Department of Neurobiology, A. I. Virtanen Institute, University of Eastern Finland) for COX8-dsRed2, and Mike Ryan (Department of Biochemistry, La Trobe University, Australia) for TOM7-GFP.

We have no conflict of interest.

REFERENCES

1. **Martin I, Dawson VL, Dawson TM.** 2011. Recent advances in the genetics of Parkinson's disease. Annu. Rev. Genomics Hum. Genet. **12:**301–325. http://dx.doi.org/10.1146/annurev-genom-082410-101440.
2. **Kitada T, Asakawa S, Hattori N, Matsumine H, Yamamura Y, Minoshima S, Yokochi M, Mizuno Y, Shimizu N.** 1998. Mutations in the parkin gene cause autosomal recessive juvenile parkinsonism. Nature **392:**605–608. http://dx.doi.org/10.1038/33416.
3. **Valente EM, Abou-Sleiman PM, Caputo V, Muqit MM, Harvey K, Gispert S, Ali Z, Del Turco D, Bentivoglio AR, Healy DG, Albanese A, Nussbaum R, Gonzalez-Maldonado R, Deller T, Salvi S, Cortelli P, Gilks WP, Latchman DS, Harvey RJ, Dallapiccola B, Auburger G, Wood NW.** 2004. Hereditary early-onset Parkinson's disease caused by mutations in PINK1. Science **304:**1158–1160. http://dx.doi.org/10.1126/science.1096284.
4. **Bonifati V, Rizzu P, van Baren MJ, Schaap O, Breedveld GJ, Krieger E, Dekker MC, Squitieri F, Ibanez P, Joosse M, van Dongen JW, Vanacore N, van Swieten JC, Brice A, Meco G, van Duijn CM, Oostra BA, Heutink P.** 2003. Mutations in the DJ-1 gene associated with autosomal recessive early-onset parkinsonism. Science **299:**256–259. http://dx.doi.org/10.1126/science.1077209.
5. **Olzmann JA, Bordelon JR, Muly EC, Rees HD, Levey AI, Li L, Chin LS.** 2007. Selective enrichment of DJ-1 protein in primate striatal neuronal processes: implications for Parkinson's disease. J. Comp. Neurol. **500:**585–599. http://dx.doi.org/10.1002/cne.21191.
6. **Andres-Mateos E, Perier C, Zhang L, Blanchard-Fillion B, Greco TM, Thomas B, Ko HS, Sasaki M, Ischiropoulos H, Przedborski S, Dawson TM, Dawson VL.** 2007. DJ-1 gene deletion reveals that DJ-1 is an atypical peroxiredoxin-like peroxidase. Proc. Natl. Acad. Sci. U. S. A. **104:**14807–14812. http://dx.doi.org/10.1073/pnas.0703219104.
7. **Canet-Aviles RM, Wilson MA, Miller DW, Ahmad R, McLendon C, Bandyopadhyay S, Baptista MJ, Ringe D, Petsko GA, Cookson MR.** 2004. The Parkinson's disease protein DJ-1 is neuroprotective due to cysteine-sulfinic acid-driven mitochondrial localization. Proc. Natl. Acad. Sci. U. S. A. **101:**9103–9108. http://dx.doi.org/10.1073/pnas.0402959101.
8. **Mitsumoto A, Nakagawa Y, Takeuchi A, Okawa K, Iwamatsu A, Takanezawa Y.** 2001. Oxidized forms of peroxiredoxins and DJ-1 on two-dimensional gels increased in response to sublethal levels of paraquat. Free Radic. Res. **35:**301–310. http://dx.doi.org/10.1080/10715760100300831.
9. **Taira T, Saito Y, Niki T, Iguchi-Ariga SM, Takahashi K, Ariga H.** 2004. DJ-1 has a role in antioxidative stress to prevent cell death. EMBO Rep. **5:**213–218. http://dx.doi.org/10.1038/sj.embor.7400074.
10. **Martinat C, Shendelman S, Jonason A, Leete T, Beal MF, Yang L, Floss T, Abeliovich A.** 2004. Sensitivity to oxidative stress in DJ-1-deficient dopamine neurons: an ES- derived cell model of primary Parkinsonism. PLoS Biol. **2:**e327. http://dx.doi.org/10.1371/journal.pbio.0020327.
11. **Menzies FM, Yenisetti SC, Min KT.** 2005. Roles of Drosophila DJ-1 in survival of dopaminergic neurons and oxidative stress. Curr. Biol. **15:**1578–1582. http://dx.doi.org/10.1016/j.cub.2005.07.036.
12. **Kim RH, Smith PD, Aleyasin H, Hayley S, Mount MP, Pownall S, Wakeham A, You-Ten AJ, Kalia SK, Horne P, Westaway D, Lozano AM, Anisman H, Park DS, Mak TW.** 2005. Hypersensitivity of DJ-1-deficient mice to 1-methyl-4-phenyl-1,2,3,6-tetrahydropyrindine (MPTP) and oxidative stress. Proc. Natl. Acad. Sci. U. S. A. **102:**5215–5220. http://dx.doi.org/10.1073/pnas.0501282102.
13. **Meulener MC, Xu K, Thomson L, Ischiropoulos H, Bonini NM.** 2006. Mutational analysis of DJ-1 in Drosophila implicates functional inactivation by oxidative damage and aging. Proc. Natl. Acad. Sci. U. S. A. **103:**12517–12522. http://dx.doi.org/10.1073/pnas.0601891103.
14. **Inden M, Taira T, Kitamura Y, Yanagida T, Tsuchiya D, Takata K, Yanagisawa D, Nishimura K, Taniguchi T, Kiso Y, Yoshimoto K, Agatsuma T, Koide-Yoshida S, Iguchi-Ariga SM, Shimohama S, Ariga H.** 2006. PARK7 DJ-1 protects against degeneration of nigral dopaminergic neurons in Parkinson's disease rat model. Neurobiol. Dis. **24:**144–158. http://dx.doi.org/10.1016/j.nbd.2006.06.004.
15. **Kinumi T, Kimata J, Taira T, Ariga H, Niki E.** 2004. Cysteine-106 of DJ-1 is the most sensitive cysteine residue to hydrogen peroxide-mediated oxidation in vivo in human umbilical vein endothelial cells. Biochem. Biophys. Res. Commun. **317:**722–728. http://dx.doi.org/10.1016/j.bbrc.2004.03.110.
16. **Nagakubo D, Taira T, Kitaura H, Ikeda M, Tamai K, Iguchi-Ariga SM, Ariga H.** 1997. DJ-1, a novel oncogene which transforms mouse NIH3T3 cells in cooperation with ras. Biochem. Biophys. Res. Commun. **231:**509–513. http://dx.doi.org/10.1006/bbrc.1997.6132.
17. **Zhang L, Shimoji M, Thomas B, Moore DJ, Yu SW, Marupudi NI, Torp R, Torgner IA, Ottersen OP, Dawson TM, Dawson VL.** 2005. Mitochondrial localization of the Parkinson's disease related protein DJ-1: implications for pathogenesis. Hum. Mol. Genet. **14:**2063–2073. http://dx.doi.org/10.1093/hmg/ddi211.
18. **Junn E, Jang WH, Zhao X, Jeong BS, Mouradian MM.** 2009. Mitochondrial localization of DJ-1 leads to enhanced neuroprotection. J. Neurosci. Res. **87:**123–129. http://dx.doi.org/10.1002/jnr.21831.
19. **Hayashi T, Ishimori C, Takahashi-Niki K, Taira T, Kim YC, Maita H, Maita C, Ariga H, Iguchi-Ariga SM.** 2009. DJ-1 binds to mitochondrial

complex I and maintains its activity. Biochem. Biophys. Res. Commun. **390:**667–672. http://dx.doi.org/10.1016/j.bbrc.2009.10.025.
20. **Maita C, Maita H, Iguchi-Ariga SM, Ariga H.** 2013. Monomer DJ-1 and its N-terminal sequence are necessary for mitochondrial localization of DJ-1 mutants. PLoS One **8:**e54087. http://dx.doi.org/10.1371/journal.pone.0054087.
21. **van der Brug MP, Blackinton J, Chandran J, Hao LY, Lal A, Mazan-Mamczarz K, Martindale J, Xie C, Ahmad R, Thomas KJ, Beilina A, Gibbs JR, Ding J, Myers AJ, Zhan M, Cai H, Bonini NM, Gorospe M, Cookson MR.** 2008. RNA binding activity of the recessive parkinsonism protein DJ-1 supports involvement in multiple cellular pathways. Proc. Natl. Acad. Sci. U. S. A. **105:**10244–10249. http://dx.doi.org/10.1073/pnas.0708518105.
22. **Blackinton J, Lakshminarasimhan M, Thomas KJ, Ahmad R, Greggio E, Raza AS, Cookson MR, Wilson MA.** 2009. Formation of a stabilized cysteine sulfinic acid is critical for the mitochondrial function of the parkinsonism protein DJ-1. J. Biol. Chem. **284:**6476–6485. http://dx.doi.org/10.1074/jbc.M806599200.
23. **Junn E, Taniguchi H, Jeong BS, Zhao X, Ichijo H, Mouradian MM.** 2005. Interaction of DJ-1 with Daxx inhibits apoptosis signal-regulating kinase 1 activity and cell death. Proc. Natl. Acad. Sci. U. S. A. **102:**9691–9696. http://dx.doi.org/10.1073/pnas.0409635102.
24. **Takahashi K, Taira T, Niki T, Seino C, Iguchi-Ariga SM, Ariga H.** 2001. DJ-1 positively regulates the androgen receptor by impairing the binding of PIASx alpha to the receptor. J. Biol. Chem. **276:**37556–37563. http://dx.doi.org/10.1074/jbc.M101730200.
25. **Niki T, Takahashi-Niki K, Taira T, Iguchi-Ariga SM, Ariga H.** 2003. DJBP: a novel DJ-1-binding protein, negatively regulates the androgen receptor by recruiting histone deacetylase complex, and DJ-1 antagonizes this inhibition by abrogation of this complex. Mol. Cancer Res. **1:**247–261. http://mcr.aacrjournals.org/content/1/4/247.
26. **Clements CM, McNally RS, Conti BJ, Mak TW, Ting JP.** 2006. DJ-1, a cancer- and Parkinson's disease-associated protein, stabilizes the antioxidant transcriptional master regulator Nrf2. Proc. Natl. Acad. Sci. U. S. A. **103:**15091–15096. http://dx.doi.org/10.1073/pnas.0607260103.
27. **Shinbo Y, Taira T, Niki T, Iguchi-Ariga SM, Ariga H.** 2005. DJ-1 restores p53 transcription activity inhibited by Topors/p53BP3. Int. J. Oncol. **26:**641–648. http://dx.doi.org/10.3892/ijo.26.3.641.
28. **Kato I, Maita H, Takahashi-Niki K, Saito Y, Noguchi N, Iguchi-Ariga SM, Ariga H.** 2013. Oxidized DJ-1 inhibits p53 by sequestering p53 from promoters in a DNA-binding affinity-dependent manner. Mol. Cell. Biol. **33:**340–359. http://dx.doi.org/10.1128/MCB.01350-12.
29. **Zhong N, Kim CY, Rizzu P, Geula C, Porter DR, Pothos EN, Squitieri F, Heutink P, Xu J.** 2006. DJ-1 transcriptionally up-regulates the human tyrosine hydroxylase by inhibiting the sumoylation of pyrimidine tract-binding protein-associated splicing factor. J. Biol. Chem. **281:**20940–20948. http://dx.doi.org/10.1074/jbc.M601935200.
30. **Ishikawa S, Taira T, Takahashi-Niki K, Niki T, Ariga H, Iguchi-Ariga SM.** 2010. Human DJ-1-specific transcriptional activation of tyrosine hydroxylase gene. J. Biol. Chem. **285:**39718–39731. http://dx.doi.org/10.1074/jbc.M110.137034.
31. **Moore DJ, Zhang L, Dawson TM, Dawson VL.** 2003. A missense mutation (L166P) in DJ-1, linked to familial Parkinson's disease, confers reduced protein stability and impairs homo-oligomerization. J. Neurochem. **87:**1558–1567. http://dx.doi.org/10.1111/j.1471-4159.2003.02265.x.
32. **Chandran JS, Lin X, Zapata A, Hoke A, Shimoji M, Moore SO, Galloway MP, Laird FM, Wong PC, Price DL, Bailey KR, Crawley JN, Shippenberg T, Cai H.** 2008. Progressive behavioral deficits in DJ-1-deficient mice are associated with normal nigrostriatal function. Neurobiol Dis. **29:**505–514. http://dx.doi.org/10.1016/j.nbd.2007.11.011.
33. **Johnston AJ, Hoogenraad J, Dougan DA, Truscott KN, Yano M, Mori M, Hoogenraad NJ, Ryan MT.** 2002. Insertion and assembly of human tom7 into the preprotein translocase complex of the outer mitochondrial membrane. J. Biol. Chem. **277:**42197–42204. http://dx.doi.org/10.1074/jbc.M205613200.
34. **Bjorkblom B, Ostman N, Hongisto V, Komarovski V, Filen JJ, Nyman TA, Kallunki T, Courtney MJ, Coffey ET.** 2005. Constitutively active cytoplasmic c-Jun N-terminal kinase 1 is a dominant regulator of dendritic architecture: role of microtubule-associated protein 2 as an effector. J. Neurosci. **25:**6350–6361. http://dx.doi.org/10.1523/JNEUROSCI.1517-05.2005.
35. **Bjorkblom B, Vainio JC, Hongisto V, Herdegen T, Courtney MJ, Coffey ET.** 2008. All JNKs can kill, but nuclear localization is critical for neuronal death. J. Biol. Chem. **283:**19704–19713. http://dx.doi.org/10.1074/jbc.M707744200.
36. **Waetzig V, Wacker U, Haeusgen W, Bjorkblom B, Courtney MJ, Coffey ET, Herdegen T.** 2009. Concurrent protective and destructive signaling of JNK2 in neuroblastoma cells. Cell. Signal. **21:**873–880. http://dx.doi.org/10.1016/j.cellsig.2009.01.032.
37. **Xia Z, Dudek H, Miranti CK, Greenberg ME.** 1996. Calcium influx via the NMDA receptor induces immediate early gene transcription by a MAP kinase/ERK-dependent mechanism. J. Neurosci. **16:**5425–5436.
38. **Coffey ET, Hongisto V, Dickens M, Davis RJ, Courtney MJ.** 2000. Dual roles for c-Jun N-terminal kinase in developmental and stress responses in cerebellar granule neurons. J. Neurosci. **20:**7602–7613.
39. **Vonsattel JP, Del Amaya MP, Keller CE.** 2008. Twenty-first century brain banking. Processing brains for research: the Columbia University methods. Acta Neuropathol. **115:**509–532. http://dx.doi.org/10.1007/s00401-007-0311-9.
40. **Burgoyne RD, Cambray-Deakin MA.** 1988. The cellular neurobiology of neuronal development: the cerebellar granule cell. Brain Res. **472:**77–101.
41. **Macedo MG, Anar B, Bronner IF, Cannella M, Squitieri F, Bonifati V, Hoogeveen A, Heutink P, Rizzu P.** 2003. The DJ-1L166P mutant protein associated with early onset Parkinson's disease is unstable and forms higher-order protein complexes. Hum. Mol. Genet. **12:**2807–2816. http://dx.doi.org/10.1093/hmg/ddg304.
42. **Blackinton J, Ahmad R, Miller DW, van der Brug MP, Canet-Aviles RM, Hague SM, Kaleem M, Cookson MR.** 2005. Effects of DJ-1 mutations and polymorphisms on protein stability and subcellular localization. Brain Res. Mol. Brain Res. **134:**76–83. http://dx.doi.org/10.1016/j.molbrainres.2004.09.004.
43. **Lange A, Mills RE, Lange CJ, Stewart M, Devine SE, Corbett AH.** 2007. Classical nuclear localization signals: definition, function, and interaction with importin alpha. J. Biol. Chem. **282:**5101–5105. http://dx.doi.org/10.1074/jbc.R600026200.
44. **Lee BJ, Cansizoglu AE, Suel KE, Louis TH, Zhang Z, Chook YM.** 2006. Rules for nuclear localization sequence recognition by karyopherin beta 2. Cell **126:**543–558. http://dx.doi.org/10.1016/j.cell.2006.05.049.
45. **Kumaran R, Vandrovcova J, Luk C, Sharma S, Renton A, Wood NW, Hardy JA, Lees AJ, Bandopadhyay R.** 2009. Differential DJ-1 gene expression in Parkinson's disease. Neurobiol Dis. **36:**393–400. http://dx.doi.org/10.1016/j.nbd.2009.08.011.
46. **Joselin AP, Hewitt SJ, Callaghan SM, Kim RH, Chung YH, Mak TW, Shen J, Slack RS, Park DS.** 2012. ROS-dependent regulation of Parkin and DJ-1 localization during oxidative stress in neurons. Hum. Mol. Genet. **21:**4888–4903. http://dx.doi.org/10.1093/hmg/dds325.
47. **Tao X, Tong L.** 2003. Crystal structure of human DJ-1, a protein associated with early onset Parkinson's disease. J. Biol. Chem. **278:**31372–31379. http://dx.doi.org/10.1074/jbc.M304221200.
48. **Lakshminarasimhan M, Maldonado MT, Zhou W, Fink AL, Wilson MA.** 2008. Structural impact of three Parkinsonism-associated missense mutations on human DJ-1. Biochemistry **47:**1381–1392. http://dx.doi.org/10.1021/bi701189c.
49. **Hulleman JD, Mirzaei H, Guigard E, Taylor KL, Ray SS, Kay CM, Regnier FE, Rochet JC.** 2007. Destabilization of DJ-1 by familial substitution and oxidative modifications: implications for Parkinson's disease. Biochemistry **46:**5776–5789. http://dx.doi.org/10.1021/bi7001778.
50. **Repici M, Straatman KR, Balduccio N, Enguita FJ, Outeiro TF, Giorgini F.** 2013. Parkinson's disease-associated mutations in DJ-1 modulate its dimerization in living cells. J. Mol. Med. **91:**599–611. http://dx.doi.org/10.1007/s00109-012-0976-y.
51. **Hu CD, Kerppola TK.** 2003. Simultaneous visualization of multiple protein interactions in living cells using multicolor fluorescence complementation analysis. Nat. Biotechnol. **21:**539–545. http://dx.doi.org/10.1038/nbt816.
52. **Xiong H, Wang D, Chen L, Choo YS, Ma H, Tang C, Xia K, Jiang W, Ronai Z, Zhuang X, Zhang Z.** 2009. Parkin, PINK1, and DJ-1 form a ubiquitin E3 ligase complex promoting unfolded protein degradation. J. Clin. Invest. **119:**650–660. http://dx.doi.org/10.1172/JCI37617.
53. **Hao LY, Giasson BI, Bonini NM.** 2010. DJ-1 is critical for mitochondrial function and rescues PINK1 loss of function. Proc. Natl. Acad. Sci. U. S. A. **107:**9747–9752. http://dx.doi.org/10.1073/pnas.0911175107.
54. **Annesi G, Savettieri G, Pugliese P, D'Amelio M, Tarantino P, Ragonese P, La Bella V, Piccoli T, Civitelli D, Annesi F, Fierro B, Piccoli F, Arabia**

G, Caracciolo M, Ciro Candiano IC, Quattrone A. 2005. DJ-1 mutations and Parkinsonism-dementia-amyotrophic lateral sclerosis complex. Ann. Neurol. **58:**803–807. http://dx.doi.org/10.1002/ana.20666.

55. **Saitoh M, Nishitoh H, Fujii M, Takeda K, Tobiume K, Sawada Y, Kawabata M, Miyazono K, Ichijo H.** 1998. Mammalian thioredoxin is a direct inhibitor of apoptosis signal-regulating kinase (ASK) 1. EMBO J. **17:**2596–2606. http://dx.doi.org/10.1093/emboj/17.9.2596.
56. **Im JY, Lee KW, Junn E, Mouradian MM.** 2010. DJ-1 protects against oxidative damage by regulating the thioredoxin/ASK1 complex. Neurosci. Res. **67:**203–208. http://dx.doi.org/10.1016/j.neures.2010.04.002.
57. **Kim SJ, Park YJ, Hwang IY, Youdim MB, Park KS, Oh YJ.** 2012. Nuclear translocation of DJ-1 during oxidative stress-induced neuronal cell death. Free Radic. Biol. Med. **53:**936–950. http://dx.doi.org/10.1016/j.freeradbiomed.2012.05.035.